(27) B. A. Averill, T. Herskovitz, R. H. Holm, and J. A. Ibers, *J. Am. Chem. Soc.*, **95**, 3523 (1973).
(28) J. J. Mayerle, S. E. Denmark, B. V. DePamphilis, J. A. Ibers, and R. H. Holm, *J. Am. Chem. Soc.*, **97**, 1032 (1975).
(29) B. V. DePamphilis, B. A. Averill, T. Herskovitz, L. Que, Jr., and R. H. Holm, *J. Am. Chem. Soc.*, **96**, 4159 (1974).
(30) D. F. Evans, *J. Chem. Soc.*, 2003 (1959).
(31) E. W. Washburn, Ed., "International Critical Tables of Numerical Data, Physics, Chemistry, and Technology", Vol. III, McGraw-Hill, New York, N.Y., 1928.
(32) J. Baudet, *J. Chim. Phys. Phys.-Chim. Biol.*, **58**, 228 (1961).
(33) L. Que, Jr., M. A. Bobrik, J. A. Ibers, and R. H. Holm, *J. Am. Chem. Soc.*, **96**, 4168 (1974).
(34) (a) M. Cerdonio, R.-H. Wang, J. Rawlings, and H. B. Gray, *J. Am. Chem. Soc.*, **96**, 6534 (1974); (b) B. C. Antanaitis and T. H. Moss, *Biochim. Biophys. Acta*, **405**, 262 (1975).
(35) The dianion *m*-H and *p*-H signal splittings in Figures 3 and 4 are due to spin–spin coupling as judged from their temperature and frequency invariant separations of 6–7 Hz. The two inequivalent *o*-H signals are resolved in the spectrum of $[Fe_4S_4(S\text{-}m\text{-}tol)_4]^{2-}$ (Figure 4).
(36) R. H. Holm and C. J. Hawkins in "NMR of Paramagnetic Molecules: Principles and Applications", G. N. La Mar, W. D. Horrocks, and R. H. Holm, Ed., Academic Press, New York, N.Y., 1973, Chapter 7.
(37) J. P. Jesson in "NMR of Paramagnetic Molecules: Principles and Applications", G. N. La Mar, W. D. Horrocks, and R. H. Holm, Ed., Academic Press, New York, N.Y., 1973, Chapter 1.
(38) G. N. La Mar, G. R. Eaton, R. H. Holm, and F. A. Walker, *J. Am. Chem. Soc.*, **95**, 63 (1973).
(39) W. E. Hatfield in "Theory and Applications of Molecular Paramagnetism", E. A. Boudreaux and L. N. Mulay, Ed., Wiley, New York, N.Y., 1976, Chapter 7.
(40) K. S. Murray, *Coord. Chem. Rev.*, **12**, 1 (1974).
(41) W. D. Horrocks, Jr., in ref 37, Chapter 4.
(42) The following data (T(K), $10^3\chi_t$ (cgs/mol), $\mu_t(\mu_B)$) were obtained for Et_4N^+ salts: $[Fe_4S_4(SPh)_4]^{2-}$, 50.2, 0.440, 0.42; 100.2, 0.631, 0.71; 220.4, 1.66, 1.71; 299.1, 1.97, 2.17; 338.1, 2.10, 2.38; $[Fe_4S_4(SPh)_4]^{3-}$, 50.2, 17.4, 2.64; 100.2, 11.5, 3.03; 220.4, 8.48, 3.87; 299.1, 7.89, 4.35; 338.1, 7.63, 4.54. These values are parts of larger data sets and differ from solution values (Table III), as do solid (Table II) and solution data for $[Fe_4S_4(SCH_2Ph)_4]^{3-}$. These differences are most pronounced for the latter trianion and are believed to arise from changes in Fe_4S_4 core structures in the crystalline and solution phases. This matter will be discussed elsewhere together with a more extensive presentation of magnetic data.[22]
(43) C. Y. Yang, K. H. Johnson, R. H. Holm, and J. G. Norman, Jr., *J. Am. Chem. Soc.*, **97**, 6596 (1975); K. H. Johnson, private communication, Oct 1977.
(44) For a thorough discussion of spin delocalization mechanisms cf. G. N. La Mar in ref 37, Chapter 3.
(45) R. H. Holm, B. A. Averill, T. Herskovitz, R. B. Frankel, H. B. Gray, O. Siiman, and F. J. Grunthaner, *J. Am. Chem. Soc.*, **96**, 2644 (1974).
(46) It cannot be assumed that all α-H and β-H signals occur in these ranges.
(47) Another possibility, less consistent with the stated experimental results, is a dynamic averaging of Fe sites in the irregular $[Fe_4S_4(SCH_2Ph)_4]^{3-}$ structure at a rate fast on the ^1H NMR time scale.
(48) R. Cammack, D. P. E. Dickson, and C. E. Johnson in ref 3, Chapter 8.

Synthetic Analogues of the 4-Fe Active Sites of Reduced Ferredoxins. Electronic Properties of the Tetranuclear Trianions $[Fe_4S_4(SR)_4]^{3-}$ and the Structure of $[(C_2H_5)_3(CH_3)N]_3[Fe_4S_4(SC_6H_5)_4]$

E. J. Laskowski,[1a] R. B. Frankel,*[1b] W. O. Gillum,[1a] G. C. Papaefthymiou,[1b] J. Renaud,[1ac] James A. Ibers,*[1d] and R. H. Holm*[1a]

Contribution from the Departments of Chemistry, Stanford University, Stanford, California 94305, and Northwestern University, Evanston, Illinois 60201, and the Francis Bitter National Magnet Laboratory, Massachusetts Institute of Technology, Cambridge, Massachusetts 02139. *Received January 16, 1978*

Abstract: The electronic properties (EPR and Mössbauer spectra, magnetic susceptibilities) of the recently synthesized, reduced tetranuclear cluster salts $(R'_4N)_3[Fe_4S_4(SR)_4]$ have been investigated in detail. The collective results fully support a description of the trianions as analogues of the 4-Fe sites of reduced ferredoxin proteins (Fd_{red}). The compound $(Et_3MeN)_3[Fe_4S_4(SPh)_4]$ crystallizes in the monoclinic space group C_s^4-Cc with 8 formula units in a cell of dimensions a = 11.426 (5), b = 24.806 (7), c = 39.147 (10) Å, and β = 90.75 (2)°. The two crystallographically independent trianions have virtually identical structures which resemble that of $[Fe_4S_4(SPh)_4]^{2-}$ in having Fe_4S_4 core configurations of idealized D_{2d} symmetry, but differ in that the cores are elongated rather than compressed along the $\bar{4}$ axis. Trianions exhibit axial EPR spectra and temperature and power saturation characteristics similar to those of Fd_{red} proteins. Zero-field Mössbauer spectra of polycrystalline samples and acetonitrile solutions at low temperatures consist of two overlapping quadrupole doublets with parameters very similar to those of *B. stearothermophilus* Fd_{red}. Magnetic properties of polycrystalline and solution samples of $[Fe_4S_4(SR)_4]^{3-}$ are consistent with a spin-doublet ground state and appreciable population of higher spin states, arising from net antiferromagnetic spin coupling, at temperatures down to 4.2 K. A significant observation is that the appreciable differences in Mössbauer and magnetic behavior of polycrystalline samples of $[Fe_4S_4(SPh)_4]^{3-}$ and $[Fe_4S_4(SCH_2Ph)_4]^{3-}$ (whose core structure is less regular than that of the former trianion) are much attenuated when examined in frozen acetonitrile solutions. Because the properties of $[Fe_4S_4(SPh)_4]^{3-}$ are much less sensitive to phase changes, we conclude that an elongated tetragonal geometry is the intrinsically stable core structure of $[Fe_4S_4(SR)_4]^{3-}$. On this basis it is speculated that the native forms of "high-potential", but not Fd, proteins may have evolved to resist the ca. 0.08 Å axial core expansion found in passing from analogue dianion to trianion. The former proteins are reducible only in the unfolded state.

Introduction

The existence of three physiologically significant total oxidation levels of the $[Fe_4S_4(S\text{-}Cys)_4]$ clusters present in nonheme iron–sulfur redox proteins[2,3] (Fd, HP[4]) is now firmly established. Based on comparative physicochemical properties of the active sites of proteins and synthetic analogues[7] and their known one-electron redox reactions, the vertical isoelectronic relationships in series 1 have emerged. As yet no single protein

$$\underset{Fd_{red}\quad HP_{s\text{-}red}}{[Fe_4S_4(SR)_4]^{3-}} \rightleftharpoons \underset{Fd_{ox}\quad HP_{red}}{[Fe_4S_4(SR)_4]^{2-}} \rightleftharpoons \underset{Fd_{s\text{-}ox}\quad HP_{ox}}{[Fe_4S_4(SR)_4]^{-}} \quad (1)$$

in aqueous solution has been found to undergo *reversible* electron transfer encompassing all three oxidation levels. Although evidence has been presented for the existence of the $Fd_{s\text{-}ox}/Fd_{ox}$ (1 − /2 −) couples in proteins from *Azotobacter*

0002-7863/78/1500-5322$01.00/0

vinelandii,[5a] *Phodospirillum rubrum*,[5b] and *Desulfovibrio gigas*[6] and attainment of the $Fd_{s\text{-}ox}$ level by chemical oxidation of clostridial Fd_{ox},[8] the great majority of bacterial ferredoxins function as electron carriers by utilization of the Fd_{ox}/Fd_{red} (2 − /3 −) couple. The presumed physiologically significant oxidation levels of "high-potential" proteins from photosynthetic bacteria (notably *Chromatium*) are HP_{red} (2−) and HP_{ox} (1−). The $HP_{s\text{-}red}$ (3−) level has been observed only by reduction of HP_{red} in a medium capable of unfolding protein tertiary structure.[9]

An ultimately complete development of the chemistry of synthetic analogues of protein 4-Fe sites requires isolation and full structural, physicochemical, and reactivity characterization of all the three species $[Fe_4S_4(SR)_4]^{3-,2-,-}$. Tetranuclear dianions have been the most extensively investigated[7] for several reasons. They are directly and easily accessible from the anaerobic reaction of Fe(III) salts, sulfide, and thiolate[10] and are the first analogues of any type of iron-sulfur protein site to have been prepared.[10a] The isoelectronic relationships of series 1 show that the 2− oxidation level is necessarily involved in all known redox reactions of Fd and HP proteins and for this reason is of particular importance. Among properties delineated for tetranuclear dianion analogues are precise structures. The species $[Fe_4S_4(SCH_2Ph)_4]^{2-}$,[10] $[Fe_4S_4(SPh)_4]^{2-}$,[11] and $[Fe_4S_4(SCH_2CH_2CO_2)_4]^{6-}$,[12] as well as $[Fe_4S_4Cl_4]^{2-}$ [13] and $[Fe_4Se_4(SPh)_4]^{2-}$,[14] all contain isoelectronic $[Fe_4S_4]^{2+}$ or $[Fe_4Se_4]^{2+}$ cores and an overall cubane-type geometry I consistently distorted by compression

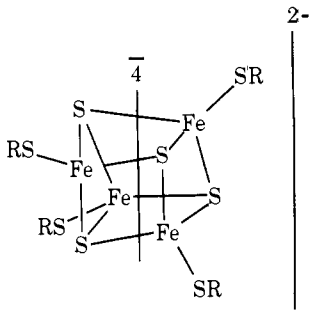

I

along the $\bar{4}$ asix toward idealized (noncrystallographically imposed) D_{2d} symmetry. Core geometries of analogues and Fd_{ox} and HP_{red} protein sites are virtually congruent.[3,7]

Species of the type $[Fe_4S_4(SR)_4]^-$ have been detected electrochemically[15] but are apparently of limited stability and numerous attempts to generate and isolate them from oxidation reactions of dianions have failed. Prior work has shown that anaerobic electrochemical[15] or chemical[16] reduction of dianions allows generation of stable trianions in solution. Electronic, Mössbauer, and EPR spectroscopic measurements of such solutions have provided reasonable proof of the isoelectronic relationship $[Fe_4S_4(SR)_4]^{3-} \equiv Fd_{red}$.[16,17] Recently the reaction

$$[Fe_4S_4(SR)_4]^{2-} + C_{12}H_8 \cdot \xrightarrow[Ar]{HMPA} [Fe_4S_4(SR)_4]^{3-} + C_{12}H_8 \quad (2)$$

employing sodium acenaphthylenide as the reducing agent, has been developed as an effective route to trianions with R = Ph and CH_2Ph.[18,19] These complexes are isolated in good yield as analytically pure, quaternary ammonium salts. Their isolation provides the means for a more rigorous comparison of analogue and protein site physicochemical properties and the first determination, in a protein or analogue, of the detailed stereochemistry of the cluster trianion oxidation level. The latter information, in conjunction with cluster dianion results,[10-12] permits an assessment of stereochemical changes pursuant to electron transfer. Previously such information has been available for only two cases: the $Rd_{ox,red}$ analogues $[Fe(S_2\text{-}o\text{-}xyl)_2]^{-,2-}$ [20] and *Chromatium* $HP_{ox,red}$.[3b,21] This report presents a detailed stereochemical description of $[Fe_4S_4(SPh)_4]^{3-}$ in its Et_3MeN^+ salt and EPR, Mössbauer, and magnetic susceptibility results for R = Ph and CH_2Ph trianions which provide the basis for a comparison of electronic structures and electron delocalization of isoelectronic analogues and protein sites.

Experimental Section

Preparation of Compounds. A. Salts of $[Fe_4S_4(SR)_4]^{2-}$. The following compounds were prepared by the method of direct tetramer synthesis as described elsewhere[10b] and were obtained after recrystallization from acetonitrile/THF as well-formed red-black crystals. $(n\text{-}Pr_4N)_2[Fe_4S_4(SPh)_4]$ was not analyzed prior to its use in the synthesis of the corresponding trianion salt.

$(Et_3MeN)_2[Fe_4S_4(SPh)_4]$. Anal. Calcd for $C_{38}H_{56}Fe_4N_2S_8$: C, 44.71; H, 5.53; N, 2.74. Found: C, 44.88; H, 5.23; N, 2.80.

$(n\text{-}Pr_4N)_2[Fe_4S_4(SCH_2Ph)_4]$. Anal. Calcd for $C_{52}H_{84}Fe_4N_2S_8$: C, 51.31; H, 6.96; N, 2.30. Found: C, 51.56; H, 7.18; N, 2.24.

B. Salts of $[Fe_4S_4(SR)_4]^{3-}$. $(Et_4N)_3[Fe_4S_4(SCH_2Ph)_4]$[18] and the following compounds were obtained by reduction of the corresponding dianion salt with sodium acenaphthylenide in HMPA solution under rigorously anaerobic conditions.[18,19] All compounds were purified by recrystallization from acetonitrile/THF and obtained as very air-sensitive black solids. Crystals of a salt of $[Fe_4S_4(SPh)_4]^{3-}$ suitable for a single-crystal x-ray diffraction investigation were obtained after a considerable search involving variation of quaternary cations and recrystallization conditions. Eventually, acceptable crystals of $(Et_3MeN)_3[Fe_4S_4(SPh)_4]$ were obtained by the following procedure.

$(Et_3MeN)_3[Fe_4S_4(SPh)_4]$. Small crystals fromthe initial crystallization were dissolved in a minimum amount of acetonitrile at 50 °C. An equal volume of warm THF was quickly added, leading to some black deposit on the walls of the flask. The solution was maintained at 30 °C for 1 day, slowly cooled to −20 °C, and allowed to stand at this temperature for 2 days. The large, black crystals present at this point were collected by filtration and washed with THF. Anal. Calcd for $C_{45}H_{74}Fe_4N_3S_8$: C, 47.54; H, 6.56; Fe, 19.65; N, 3.70; S, 22.56. Found: C, 47.81; H, 6.77; Fe, 19.30; N, 3.85; S, 21.94.

$(n\text{-}Pr_4N)_3[Fe_4S_4(SPh)_4]$. Anal. Calcd for $_{60}H_{104}Fe_4N_3S_8$: C, 53.48; H, 7.78; Fe, 16.58; N, 3.12. Found: C, 52.77; H, .16; Fe, 16.59; N, 2.74.

$(n\text{-}Pr_4N)_3Fe_4S_4(SCH_2Ph)_4]$. Anal. Calcd for $C_{64}H_{112}Fe_4N_3S_8$: C, 54.77; H, 8.04; Fe, 15.92; N, 2.99; S, 18.28. Found: C, 54.62; H, 8.31; Fe, 15.59; N, 2.55; S, 18.39.

Crystal Structure Determination. In an inert atmosphere box a black crystal of $(Et_3MeN)_3[Fe_4S_4(SPh)_4]$ was sealed in a soft-glass capillary. Pertinent details on crystal data and collection of intensity data are given in Table I and below. Particulars on methods employed, computer programs used, sources of atomic scattering factors, and related matters have been given previously for related structures.[10,11]

Structure Solution. On the basis of the observed extinctions the compound crystallizes either in the centrosymmetric space group $C_{2h}^6 - C2/c$ or in the noncentrosymmetric space group $C_s^4 - Cc$. Because $C2/c$ is the more common space group andthere are eight formula units in the cell, it was anticipated that there would be three independent cations and one independent anion to be located. However, an origin-removed three-dimensional Patterson function could not be interpreted on this basis. Instead a solution involving six independent cations and two independent anions in space group Cc was found using the MULTAN set of direct methods programs. Fromssubsequent least-squares and difference Fourier calculations the atoms of the two anions were located with ease as were the six independent nitrogen atoms and some of the carbon atoms of the cations. With a good trial structure in hand isotropic refinement of the correct enantiomeric structure (established by comparing least-squares refinements and individual Friedel pairs) converged to values of 8.1% for the R index on F for the 384 variables and 4736 data above 3σ. This refinement was on 72 individual atoms and 8 rigid phenyl groups. Although all carbon atoms of the cations were located at this stage on difference Fourier maps, some of these refined poorly yielding high thermal parameters and unreasonable N-C or C-C distances. All subsequent

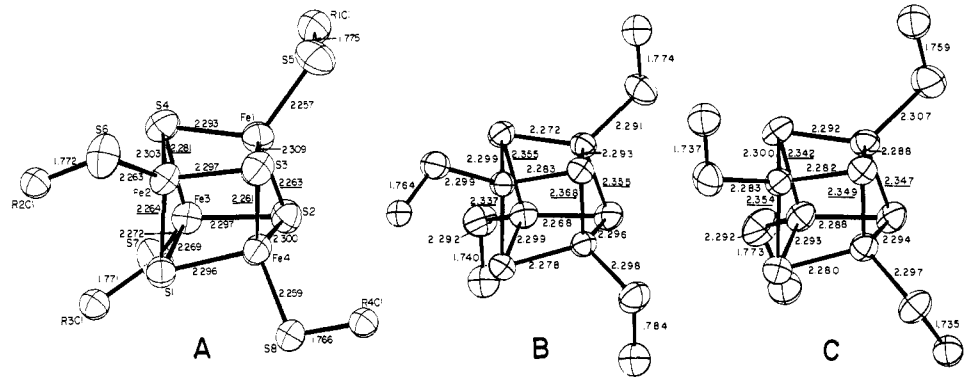

Figure 1. Structures of $[Fe_4S_4(SPh)_4]^{2-}$ [11] (A) and the two independent $[Fe_4S_4(SPh)_4]^{3-}$ anions (B, C). The atom labeling scheme of A applies to B and C, which are anions 1 and 2, respectively, in Table IV. Phenyl rings are omitted; 50% probability ellipsoids are shown.

Table I. Summary of Crystal Data and Intensity Collection for $(Et_3MeN)_3[Fe_4S_4(SPh)_4]$

formula	$C_{45}H_{74}Fe_4N_3S_8$
mol wt, amu	1137.01
a, Å	11.426 (5)
b, Å	24.806 (7)
c, Å	39.147 (10)
β, deg	90.75 (2)
V, Å^3	11 095
Z	8
d_{calcd}, g/cm^3	1.361[b]
space group	C_s^4-Cc
crystal dimensions, mm	0.6 × 0.4 × 0.3
crystal volume, mm^3	0.086
μ, cm^{-1}	112.9
transmission factors	0.043–0.187
bounding planes	{001}, {02$\bar{1}$}, (110), ($\bar{1}$05), (1$\bar{1}$2)
radiation	Cu K$\bar{\alpha}$ prefiltered and postfiltered with 1-mil Ni foils (Cu used because of length of c axis)
takeoff angle, deg	3.3
aperture	2.5 mm wide by 4.2 mm high, 32 cm from crystal
scan speed	2 deg/min
scan range	0.9 below Kα_1 to 0.8 above Kα_2
2θ range, deg	3–100°
background counts	10 s for 2θ < 85° 20 s for 2θ > 85°
data collected[a]	$+h +k +l$, with Friedel pairs below 40°
unique data	5736 (ignoring Friedel pairs)
p factor	0.03

[a] Six standards showed an average decline of 2.5% by the end of data collection. [b] Experimental density not determined because of air sensitivity of the compound.

attempts to define these atoms more precisely failed, leading to the conclusion that several of the Et_3MeN^+ cations are disordered. At this point a computer analysis was made of the 64 iron atom positions in the cell in the form of a search for an origin shift that would relate 32 of these positions to the other 32 by a center of symmetry. No such center could be found. This result together with the analysis of Friedel pairs provides convincing evidence that the correct space group is $C_s^4 - Cc$.

Structure **Refinement.** Refinement proceeded by usual methods. Owing to the unsatisfactory behavior of some of the cation carbon atoms during isotropic refinement, anisotropic refinement was limited to the 8 iron and 16 sulfur atoms of the two inequivalent anions. Cations and rigid group phenyl atoms were refined isotropically. Refinement of 504 variables by full-matrix least-squares methods converged to R and R_w on F^2 of 0.121 and 0.156, respectively, and to an error in observation of unit weight of 2.11 e^2. In this calculation all 5736 unique (non-Friedel) reflections were employed. The conventional R index on F for $F_o^2 \geq 3\sigma(F_o^2)$ is 0.068. The last cycle of refinement included hydrogen atoms of phenyl rings and methylene groups of the cations at calculated positions. The final difference Fourier revealed maximum peaks of ca. 0.6 e/Å^3 in the vicinity of the troublesome cations. An analysis of errors clearly showed worst agreement for strong reflections at low 2θ values, as is expected in view of the difficulty in locating cation carbon atom positions.

The following results for $(Et_3MeN)_3[Fe_4S_4(SPh)_4]$ are tabulated: positional and thermal parameters for nongroup atoms (Table II), derived parameters for rigid group atoms and rigid group parameters (Table III), distances and angles in the anions (Table IV), atomic deviations from best weighted least-squares planes of the anions (Table V), equations of best weighted least-squares planes of the anions (Table VI[22]), root mean square amplitudes of vibration (Table VII), values of F_o^2 and F_c^2 (Table VIII[22]), and comparison of structural parameters of $[Fe_4S_4(SPh)_4]^{2-,3-}$ (Table IX).

Core Congruence. A means was sought to relate the core structures of the two independent $[Fe_4S_4(SPh)_4]^{3-}$ anions to each other and to compare them with the core structure of $[Fe_4S_4(SPh)_4]^{2-}$; these structures are shown in Figure 1. Considering first the problem of geometrically matching most ciosely two imperfect tetrahedra (Fe_4 or S_4*), there are 12 possible ways (orientations) in which they can be matched. A computer program was written to transform each tetrahedron to an orthonormal coordinate system and then to fit tetrahedron A to tetrahedron B by rotation and translation using the least-squares criterion that the quantity Q in eq 3 be minimized.

$$Q = \sum_{j=1}^{n} \sum_{i=2}^{3} \frac{(q_A^{ij} - q_B^{ij})^2}{\sigma^2(q_A^{ij}) + \sigma^2(q_B^{ij})} \quad (3)$$

Here n is the number of atoms and σ is the estimated standard deviation in coordinate $q = x, y, z$. It was evident early in the calculations that while Fe_4 tetrahedra in the two trianions and in the dianion and either trianion approach congruence in certain orientations, the dianion core is not congruent with either trianion core in any orientation. Thus the most noticeable changes upon passing from dianion to trianion occur in the S_4* units relative to the Fe_4 tetrahedra. Calculations were performed for each of the possible way of matching the two trianion $[Fe_4S_4*]^+$ cores and the Fe_4 tetrahedra of the dianion and each of the trianions. In each case a clearly defined minimum in Q was found, which is taken as indicative of that orientation affording maximum core or Fe_4 congruence. For these minima the following deviations in distances between proximal vertices of the two polyhedra were found. (1) $[Fe_4S_4*]^+$ cores of trianions 1 and 2: Fe···Fe, 0.008, 0.022, 0.011, 0.006 (mean 0.012 Å); S*···S*, 0.024, 0.027, 0.029, 0.012 (mean 0.023 Å). (2) Fe_4 tetrahedra of dianion and trianion 1: 0.014, 0.010, 0.006, 0.015 (mean 0.011 Å). (3) Fe_4 tetrahedra of dianion and trianion 2: 0.014, 0.013, 0.013, 0.016 (mean 0.014 Å). The maximally congruent trianion core and dianion–trianion Fe_4 orientations are those with parallel idealized $\bar{4}$ axes, and are set out in Figure 1; accordingly, the atom labeling scheme of $[Fe_4S_4(SPh)_4]^{2-}$ (A) applies to $[Fe_4S_4(SPh)_4]^{3-}$ (B, C).

Other Physical Measurements. A. EPR Spectra. Measurements were carried out at ca. 9.2 GHz using a Varian E-12 spectrometer system equipped with an Air Products Model LT-3-110 Helitran refrigerator and a Model APD-B temperature controller. Solutions of salts of $[Fe_4S_4(SR)_4]^{3-}$ were prepared under an argon atmosphere using thoroughly dired and degassed solvents, and were sealed in quartz EPR tubes under vacuum. Spectra were recorded as soon as possible after sample preparation; however, independent experiments

Table II. Positional and Thermal Parameters for the Non-Rigid-Group Atoms of $(Et_3MeN)_3[Fe_4S_4(SPh)_4]$

ATOM	X[A]	Y	Z	B11[B] OR B,A[2]	B22	B33	B12	B13	B23
FE(21)	0.14660	0.24950(11)	0.44050	76.4(28)	15.02(55)	5.78(22)	0.94(95)	2.27(68)	0.05(28)
FE(31)	0.16038(35)	0.22846(11)	0.50902(10)	90.0(29)	16.93(58)	6.23(23)	-0.3(10)	-1.36(64)	0.44(30)
FE(41)	-0.01940(34)	0.18614(11)	0.47096(10)	82.2(30)	14.82(56)	7.12(23)	-2.2(10)	2.81(63)	-0.44(31)
FE(11)	-0.00965(34)	0.29589(11)	0.48405(10)	83.7(29)	15.27(57)	6.46(23)	2.7(10)	2.81(63)	-0.28(30)
FE(12)	0.44434(35)	0.52191(11)	0.19425(10)	95.4(30)	18.20(60)	5.49(24)	4.2(10)	1.75(65)	-0.09(30)
FE(32)	0.27252(34)	0.45388(12)	0.21672(10)	93.0(31)	17.25(60)	6.73(24)	3.2(10)	-3.31(66)	-0.62(32)
FE(42)	0.43439(35)	0.49155(11)	0.26216(10)	84.8(29)	17.93(59)	5.63(22)	3.32(99)	-1.89(64)	-0.68(30)
FE(22)	0.27017(33)	0.56097(12)	0.234669(98)	84.7(31)	18.27(58)	5.88(24)	6.5(10)	1.67(64)	-0.26(30)
S(21)	-0.03073(49)	0.22552(20)	0.52388(14)	107.5(48)	18.70(95)	5.98(38)	-1.2(17)	5.8(11)	0.65(52)
S(31)	-0.05060(48)	0.25772(18)	0.43189(14)	82.7(46)	17.09(91)	6.56(36)	2.3(16)	-0.7(10)	-0.27(49)
S(41)	0.18571(48)	0.31253(19)	0.48216(14)	85.1(50)	15.81(94)	7.77(36)	-4.7(17)	2.1(10)	-0.24(49)
S(11)	0.17390(48)	0.16535(19)	0.46626(14)	86.7(49)	16.02(94)	7.97(37)	3.6(17)	2.4(10)	-0.49(50)
S(61)	0.26503(55)	0.26466(22)	0.39445(16)	125.2(56)	19.4(11)	9.76(45)	4.4(20)	13.3(13)	1.74(68)
S(71)	0.30421(56)	0.23322(23)	0.55027(16)	122.5(58)	24.2(12)	9.46(47)	-2.6(21)	-7.8(13)	1.26(62)
S(81)	-0.15537(58)	0.12300(23)	0.45397(16)	113.9(60)	21.5(12)	11.35(46)	-13.1(21)	0.9(13)	-2.58(64)
S(51)	-0.12765(54)	0.35822(22)	0.50966(15)	128.5(56)	22.6(11)	8.12(44)	15.7(20)	5.1(12)	-1.37(59)
S(12)	0.23756(50)	0.48636(20)	0.27046(15)	90.5(50)	21.5(10)	7.03(39)	1.7(17)	1.5(11)	0.89(53)
S(32)	0.46558(49)	0.57837(19)	0.24014(14)	87.5(47)	17.33(91)	6.63(36)	-0.1(17)	-0.6(10)	-0.99(49)
S(42)	0.24953(50)	0.52785(20)	0.18005(14)	109.5(50)	18.96(97)	6.42(40)	9.2(17)	-5.3(11)	0.67(52)
S(22)	0.46854(50)	0.43504(19)	0.21700(14)	104.5(51)	16.9(10)	7.06(39)	11.5(18)	-0.1(11)	-1.40(53)
S(52)	0.58480(59)	0.52235(24)	0.15244(17)	143.3(64)	29.3(13)	8.49(51)	16.5(23)	10.9(15)	0.69(69)
S(72)	0.15102(58)	0.38961(23)	0.19359(17)	132.8(64)	22.3(13)	10.83(50)	1.0(22)	-11.3(14)	-1.99(68)
S(82)	0.55095(53)	0.48602(21)	0.31028(15)	118.8(54)	20.4(11)	7.77(43)	6.2(19)	-7.5(12)	-1.36(57)
S(62)	0.13718(55)	0.62276(23)	0.25303(16)	104.7(61)	22.1(12)	10.86(46)	11.6(21)	9.2(13)	-0.69(64)
N(1)	-0.0008(15)	0.15955(69)	0.33666(44)	5.73(40)					
N(2)	0.3470(22)	0.01084(93)	-0.25771(62)	8.91(60)					
N(3)	0.0652(27)	0.2545(11)	-0.03570(76)	10.54(75)					
N(4)	0.3524(33)	0.4036(14)	0.09405(92)	11.94(90)					
N(5)	0.2295(21)	0.42976(91)	0.37752(61)	8.76(55)					
N(6)	0.0660(23)	0.3451(10)	-0.38487(66)	8.89(57)					
C(11)	0.0965(21)	0.14207(94)	0.31500(61)	7.24(58)					
C(21)	-0.1122(20)	0.12734(89)	0.32613(58)	6.41(52)					
C(31)	-0.2211(23)	0.1415(10)	0.34498(67)	8.06(66)					
C(41)	0.0254(17)	0.1473(79)	0.37364(51)	5.92(44)					
C(51)	0.0521(20)	0.08791(91)	0.38380(58)	6.68(53)					
C(61)	-0.0163(23)	0.2193(11)	0.33391(69)	8.51(67)					
C(71)	-0.0588(24)	0.2374(11)	0.29771(71)	8.33(71)					
C(12)	0.4092(35)	-0.0026(15)	-0.2137(10)	10.0(12)					
C(22)	0.2496(21)	-0.03044(95)	-0.26312(58)	6.71(53)					
C(32)	0.2945(28)	-0.0912(14)	-0.26771(85)	11.43(95)					
C(42)	0.2905(23)	0.0676(11)	-0.25561(66)	8.56(65)					
C(52)	0.3771(27)	0.1134(12)	-0.24660(76)	9.49(84)					
C(62)	0.4536(42)	0.0037(19)	-0.2755(13)	19.5(15)					
C(72)	0.4115(42)	0.0127(18)	-0.3109(13)	17.7(16)					
C(13)	0.1113(37)	0.2578(15)	-0.0765(10)	7.4(13)					
C(23)	-0.0039(27)	0.2029(12)	-0.03163(75)	11.01(76)					
C(33)	0.0784(32)	0.1485(14)	-0.04012(91)	14.0(11)					
C(43)	-0.0254(24)	0.3019(11)	-0.03234(71)	7.65(68)					
C(53)	0.0113(28)	0.3566(13)	-0.03092(83)	10.20(88)					
C(63)	0.1565(48)	0.2624(21)	-0.0175(15)	20.6(18)					
C(73)	0.1166(36)	0.2598(16)	0.0198(11)	10.6(13)					
C(14)	0.4659(45)	0.4173(20)	0.0682(13)	17.1(17)					
C(24)	0.4287(53)	0.3847(22)	0.1235(15)	26.2(20)					
C(34)	0.5196(40)	0.3503(17)	0.1304(11)	15.9(14)					
C(44)	0.2721(51)	0.3678(23)	0.0751(14)	25.9(19)					
C(54)	0.2334(55)	0.3300(27)	0.1085(18)	28.4(26)					
C(64)	0.2525(74)	0.4446(34)	0.1017(20)	27.0(33)					
C(74)	0.3577(61)	0.4848(27)	0.0938(17)	29.2(25)					
C(15)	0.2822(27)	0.3983(12)	0.34834(81)	10.56(83)					
C(25)	0.1929(31)	0.4857(15)	0.36574(93)	13.0(10)					
C(35)	0.1333(27)	0.5183(12)	0.39252(78)	10.72(79)					
C(45)	0.3426(64)	0.4317(25)	0.4045(17)	24.8(25)					
C(55)	0.4288(55)	0.4481(24)	0.4025(15)	20.3(22)					
C(65)	0.1348(44)	0.4010(17)	0.3946(12)	20.0(16)					
C(75)	0.0653(46)	0.3849(21)	0.3513(15)	16.0(17)					
C(16)	0.1457(47)	0.3195(20)	-0.3602(13)	18.6(18)					
C(26)	-0.0376(44)	0.3145(19)	-0.3920(12)	18.5(15)					
C(36)	-0.1161(46)	0.3152(20)	-0.3571(14)	15.8(18)					
C(46)	0.0506(51)	0.3938(24)	-0.3699(15)	24.9(20)					
C(56)	-0.0256(48)	0.4317(22)	-0.3926(15)	22.7(21)					
C(66)	0.1051(37)	0.3547(15)	-0.4218(10)	15.8(12)					
C(76)	0.2304(30)	0.3830(13)	-0.42084(85)	12.21(95)					

[A] ESTIMATED STANDARD DEVIATIONS IN THE LEAST SIGNIFICANT FIGURE(S) ARE GIVEN IN PARENTHESES IN THIS AND ALL SUBSEQUENT TABLES. [B] THE FORM OF THE ANISOTROPIC THERMAL ELLIPSOID IS EXP(-(B11H^2 + B22K^2 + B33L^2 + 2B12HK + 2B13HL + 2B23KL)). THE QUANTITIES GIVEN IN THE TABLE ARE THE THERMAL COEFFICIENTS × 10^4.

revealed that solutions in sealed tubes stored at liquid nitrogen temperature appear to be stable for an indefinite period of time. Spectra were recorded at modulation frequencies in the range 10^3–10^5 Hz as a check for fast passage effects, but line shapes were found to be invariant over this range.

B. Magnetic Measurements. Susceptibilities of $[Fe_4S_4(SR)_4]^{2-,3-}$

Table III. Derived Parameters for the Rigid-Group Atoms of $(Et_3MeN)_3[Fe_4S_4(SPh)_4]$

ATOM	X	Y	Z	B,Å^2	ATOM	X	Y	Z	B,Å^2
R2C1	0.3345(11)	0.21041(43)	0.37375(30)	3.80(37)	R5C1	0.5785(14)	0.58560(50)	0.13217(41(	5.85(50)
R2C2	0.3311(11(	0.15747(50)	0.38550(28)	4.74(39)	R5C2	0.6208(15)	0.58863(64)	0.09904(43)	8.91(63)
R2C3	0.3902(13(	0.11714(37)	0.36804(37)	7.94(64)	R5C3	0.6144(17)	0.63701(85(	0.08110(36)	11.89(86)
R2C4	0.4528(13)	0.12974(48)	0.33883(36)	6.34(53)	R5C4	0.5657(18)	0.68237(61)	0.09628(53)	12.6(10)
R2C5	0.4562(12(	0.18267(56)	0.32708(28)	6.47(47)	R5C5	0.5234(16)	0.67934(54)	0.12941(54)	11.36(83)
R2C6	0.3970(12)	0.22301(39)	0.34454(32)	5.63(43)	R5C6	0.5298(14)	0.63096(70)	0.14735(35)	7.27(51)
R3C1	0.3177(15)	0.17168(60)	0.57129(46)	6.06(47)	R7C1	0.1820(15)	0.32894(56)	0.21586(42)	6.83(50)
R3C2	0.2829(17)	0.12291(86)	0.55680(43)	9.47(68)	R7C2	0.2386(15)	0.32889(58)	0.24757(42)	6.99(61)
R3C3	0.2944(23)	0.07531(59)	0.57538(74)	16.3(15)	R7C3	0.2636(15)	0.28030(81)	0.26388(36)	9.53(68)
R3C4	0.3407(25)	0.0764P(82)	0.60843(71)	17.4(17)	R7C4	0.2320(18)	0.23176(58)	0.24849(52)	9.22(79)
R3C5	0.3755(20)	0.1252(12)	0.62292(43)	13.7(11)	R7C5	0.1754(18)	0.23181(56)	0.21679(52)	11.88(86)
R3C6	0.3640(17)	0.17285(79)	0.60435(49)	9.36(82)	R7C6	0.1504(15)	0.28040(79)	0.20647(35)	9.59(72)
R4C1	-0.1329(16)	0.06049(49)	0.47559(38)	6.25(46)	R8C1	0.5975(13)	0.42075(44)	0.31871(38)	4.85(43)
R4C2	-0.0218(13)	0.04124(70)	0.48401(45)	7.51(62)	R8C2	0.5652(12)	0.37616(61)	0.29916(32)	6.87(48)
R4C3	-0.0088(14)	-0.00974(79)	0.49842(50)	11.99(88)	R8C3	0.6063(16)	0.32513(48)	0.30799(43)	9.56(72)
R4C4	-0.1068(19)	-0.04148(55)	0.50441(46)	10.27(74)	R8C4	0.6796(16)	0.31868(51)	0.33637(48)	8.36(69)
R4C5	-0.2180(15)	-0.02223(68)	0.49599(47)	9.66(71)	R8C5	0.7120(14)	0.36327(74)	0.35591(37)	9.67(80)
R4C6	-0.2310(12)	0.02875(73)	0.48158(44)	8.83(70)	R8C6	0.6709(14)	0.41431(58)	0.34708(36)	6.59(59)
R1C1	-0.1445(13)	0.41726(52)	0.48449(38)	5.35(43)	R6C1	0.1548(14)	0.68516(47)	0.23375(37)	5.73(48)
R1C2	-0.1450(15)	0.41514(56)	0.44895(39)	7.87(61)	R6C2	0.0595(11)	0.72007(67)	0.23197(42)	8.17(68)
R1C3	-0.1670(17)	0.46161(79)	0.42999(32)	10.10(76)	R6C3	0.0716(14)	0.77060(60)	0.21695(47)	8.53(67)
R1C4	-0.1883(17)	0.51020(60)	0.44657(51)	10.29(79)	R6C4	0.1788(17)	0.78622(49)	0.20372(45)	9.46(78)
R1C5	-0.1878(18)	0.51233(52)	0.48210(52)	11.51(94)	R6C5	0.2741(12)	0.75131(68)	0.20550(43)	9.46(69)
R1C6	-0.1658(16)	0.46586(70)	0.50106(32)	8.60(64)	R6C6	0.2621(11)	0.70078(60)	0.22051(42)	6.69(53)

RIGID GROUP PARAMETERS

GROUP	x_C[A]	y_C	z_C	DELTA[B]	EPSILON	ETA
RING 2	0.39363(78)	0.17007(35)	0.35629(23)	2.707(10)	-2.4086(76)	-2.408(10)
RING 3	0.3292(13)	0.12408(55)	0.58986(39)	2.499(21)	2.268(14)	2.194(20)
RING 4	-0.1199(11)	0.00950(46)	0.49000(28)	-1.442(11)	3.168(11)	0.4159(98)
RING 1	-0.16640(95)	0.46373(45)	0.46553(32)	-2.955(21)	2.131(11)	-1.547(28)
RING 5	0.5721(10)	0.63398(46)	0.11423(32)	-2.361(17)	2.231(11)	-2.177(17)
RING 7	0.20699(99)	0.28035(47)	0.23218(31)	-0.697(17)	-2.280(11)	0.777(17)
RING 8	0.63859(91)	0.36972(42)	0.32754(28)	2.236(15)	2.2604(94)	2.748(15)
RING 6	0.1668(10)	0.73569(41)	0.21873(27)	1.367(10)	-2.942(10)	-0.4469(97)

[A] x_C, y_C, AND z_C ARE THE FRACTIONAL COORDINATES OF THE ORIGIN OF THE RIGID GROUP. [B] THE RIGID GROUP ORIENTATION ANGLES DELTA, EPSILON, AND ETA(RADIANS) HAVE BEEN DEFINED PREVIOUSLY: S.J. LA PLACA AND J.A. IBERS, ACTA CRYSTALLOGR., 18, 511(1965).

salts in the crystalline and frozen solution states were determined with a Superconducting Technology, Inc., SQUID-type susceptometer operating at 4.2–338 K and 2–6 kG. Temperature calibration was performed using a calibrated silicon diode placed in the sample region. Magnetic moment calibration was achieved by use of an accurately constructed solenoid and a constant current supply. By varying the current supplied to the coil, the calibration could be checked over the entire range of the instrument, thereby verifying the linearity of the detection system as well as establishing the exact relationship between detector output voltage and flux quanta change. Background diamagnetic corrections for the sample holder were made by collecting data for the helium-filled sample cell over the temperature range of interest. Data were collected on the frequently used susceptibility standard $HgCo(NCS)_4$ at a field of 2007 G and 63 temperatures in the range 4.2–338.1 K. A least-squares fit of the data to the Curie–Weiss law yielded $\chi_g = (0.004\,733)/(T + 1.00)$. The latest results for this standard have been reported by Rade.[23] Similar treatment of his data (14 points at 5.8–293 K) gave $\chi_g = (0.004\,866)/(T - 3.33)$, which is in moderate agreement with our results at high temperatures but seriously departs at low temperatures ($\lesssim$100 K). Preliminary experiments have shown χ_g of $HgCo(NCS)_4$ to be slightly field dependent. We suggest that our results are suitable for calibration of bulk magnetic devices operating near 2 kG, but additional measurements are required to obtain accurate calibration data at higher fields. Measurements of salts of $[Fe_4S_4(SR)_4]^{2-,3-}$ were performed on crystalline samples and, for trianions, on frozen acetonitrile solutions as well. In the latter case data on solutions were corrected for solvent diamagnetism by measurement of a sample cell containing pure acetonitrile. All solutions and the pure solvent were manipulated under an argon atmosphere and thoroughly degassed by freeze–thaw cycles.

C. Mössbauer Spectra. The ^{57}Fe Mössbauer spectra of polycrystalline salts of $[Fe_4S_4(SPh)_4]^{3-}$ and $[Fe_4S_4(SCH_2Ph)_4]^{3-}$ interspersed with boron nitride powder were obtained at 1.6–200 K using a constant acceleration spectrometer operating in the time mode with the source of ^{57}Co in rhodium metal maintained at room temperature. Sample temperature variation was achieved with a Janis Co. "Super-Vari-temp" Dewar system. Solutions of trianions in acetonitrile were prepared under dry, oxygen-free dinitrogen and immediately frozen in liquid dinitrogen prior to use. Comparative spectra of frozen solution and polycrystalline samples were measured at 4.2 and 77 K using a spectrometer operating in the normalized mode with the ^{57}Co in rhodium source maintained at the same temperature as the absorber. Measurements in longitudinal magnetic fields up to 80 kOe at 4.2 K were made with the source placed so that the magnetic field at the source location was always less than 1 kOe.

Results and Discussion

Structure of $(Et_3MeN)_3[Fe_4S_4(SPh)_4]$. This compound crystallizes in the monoclinic space group *Cc* and contains per asymmetric unit six independent cations and two independent anions, all of which are well separated with no unusual contacts. Shown in Figure 2 is a stereoview of the contents of the unit cell. The cations possess the expected tetrahedral geometry but several appear to be disordered, as judged by large thermal parameters (Table II) and unreasonable bond distances. The 24 independent N–C distances range from 1.27 (5) to 1.89 (4) Å and average to 1.53 Å, and the range and mean value of the 18 independent C–C distances are 1.07 (8)–1.91 (6) and 1.54 Å, respectively. Refinement of this structure proceeded to the conventional *R* index of 0.068.

In the following summary of the main features of the

Table IV. Selected Distances (Å) and Angles (deg) in the Anions of $(Et_3MeN)_3[Fe_4S_4{}^*(SPh)_4]$

	anion 1	anion 2
	Fe-S	
Fe(1)-S(5)	2.291 (6)	2.307 (7)
Fe(2)-S(6)	2.299 (6)	2.283 (6)
Fe(3)-S(7)	2.292 (7)	2.292 (7)
Fe(4)-S(8)	2.298 (7)	2.297 (6)
mean	2.295 (7)[a]	2.294 (10)
	Fe-S*	
Fe(1)-S(2)	2.355 (6)	2.347 (6)
Fe(2)-S(1)	2.337 (6)	2.354 (6)
Fe(3)-S(4)	2.355 (6)	2.342 (6)
Fe(4)-S(3)	2.368 (6)	2.349 (6)
mean	2.354 (13)	2.348 (6)
Fe(1)-S(3)	2.293 (5)	2.288 (6)
Fe(1)-S(4)	2.272 (6)	2.292 (6)
Fe(2)-S(3)	2.283 (6)	2.282 (6)
Fe(2)-S(4)	2.299 (6)	2.300 (6)
Fe(3)-S(1)	2.299 (6)	2.293 (6)
Fe(3)-S(2)	2.269 (6)	2.288 (6)
Fe(4)-S(1)	2.278 (6)	2.280 (6)
Fe(4)-S(2)	2.296 (6)	2.294 (6)
mean	2.286 (12)	2.290 (7)
	Fe···Fe	
Fe(1)-Fe(2)	2.738 (4)	2.736 (4)
Fe(1)-Fe(3)	2.735 (4)	2.743 (4)
Fe(1)-Fe(4)	2.772 (4)	2.767 (4)
Fe(2)-Fe(3)	2.735 (4)	2.748 (4)
Fe(2)-Fe(4)	2.748 (4)	2.755 (4)
Fe(3)-Fe(4)	2.732 (4)	2.715 (4)
mean	2.743 (15)	2.744 (17)
	Fe···S*	
Fe(1)-S(1)	3.925 (6)	3.930 (6)
Fe(2)-S(2)	3.910 (6)	3.926 (6)
Fe(3)-S(3)	3.907 (6)	3.898 (6)
Fe(4)-S(4)	3.936 (6)	3.928 (6)
mean	3.920 (14)	3.921 (15)
	S*···S*	
S(1)-S(2)	3.595 (7)	3.621 (7)
S(3)-S(4)	3.588 (7)	3.612 (7)
mean	3.592 (7)	3.617 (7)
S(1)-S(3)	3.681 (7)	3.673 (7)
S(1)-S(4)	3.706 (7)	3.690 (7)
S(2)-S(3)	3.693 (7)	3.669 (7)
S(2)-S(4)	3.681 (7)	3.683 (7)
mean	3.690 (12)	3.679 (10)
	Fe-S*-Fe	
Fe(2)-S(1)-Fe(4)	73.06 (17)	72.94 (18)
Fe(2)-S(1)-Fe(3)	72.31 (17)	72.50 (18)
Fe(4)-S(1)-Fe(3)	73.30 (18)	72.85 (18)
Fe(1)-S(2)-Fe(3)	72.49 (17)	72.55 (18)
Fe(1)-S(2)-Fe(4)	73.16 (18)	73.20 (17)
Fe(3)-S(2)-Fe(4)	73.52 (18)	72.69 (18)
Fe(4)-S(3)-Fe(2)	72.40 (17)	73.02 (17)
Fe(4)-S(3)-Fe(1)	72.98 (17)	73.25 (17)
Fe(2)-S(3)-Fe(1)	73.49 (17)	73.55 (18)
Fe(3)-S(4)-Fe(1)	72.43 (17)	72.55 (18)
Fe(3)-S(4)-Fe(2)	71.98 (17)	72.59 (18)
Fe(1)-S(4)-Fe(2)	73.59 (17)	73.14 (18)
mean	72.89	72.90

	anion 1	anion 2
	Fe-Fe-Fe	
Fe(4)-Fe(1)-Fe(3)	59.47 (11)	59.06 (11)
Fe(4)-Fe(1)-Fe(2)	59.81 (10)	60.09 (10)
Fe(3)-Fe(1)-Fe(2)	59.97 (11)	60.22 (11)
Fe(4)-Fe(2)-Fe(3)	59.77 (10)	59.13 (10)
Fe(4)-Fe(2)-Fe(1)	60.71 (11)	60.51 (11)
Fe(3)-Fe(2)-Fe(1)	59.95 (11)	60.01 (10)
Fe(1)-Fe(3)-Fe(2)	60.08 (10)	59.77 (11)
Fe(2)-Fe(3)-Fe(4)	60.34 (10)	60.57 (10)
Fe(1)-Fe(3)-Fe(4)	60.95 (11)	60.92 (11)
Fe(1)-Fe(4)-Fe(2)	59.47 (10)	59.39 (11)
Fe(2)-Fe(4)-Fe(3)	59.89 (11)	60.30 (11)
Fe(1)-Fe(4)-Fe(3)	59.58 (10)	60.02 (11)
mean	59.98	60.00
	S-Fe-S*	
S(5)-Fe(1)-S(2)	98.3 (2)	101.2 (2)
S(5)-Fe(1)-S(3)	123.6 (2)	119.1 (2)
S(5)-Fe(1)-S(4)	118.4 (2)	120.7 (2)
S(6)-Fe(2)-S(1)	114.2 (1)	103.2 (2)
S(6)-Fe(2)-S(3)	117.4 (2)	119.9 (2)
S(6)-Fe(2)-S(4)	109.5 (2)	118.3 (2)
S(7)-Fe(3)-S(1)	119.6 (2)	119.7 (2)
S(7)-Fe(3)-S(2)	120.3 (4)	116.6 (2)
S(7)-Fe(3)-S(4)	100.2 (2)	103.9 (2)
S(8)-Fe(4)-S(1)	118.4 (2)	116.2 (2)
S(8)-Fe(4)-S(2)	120.3 (2)	119.5 (2)
S(8)-Fe(4)-S(3)	103.2 (2)	105.5 (2)
mean	113.6	113.7
	S*-S*-S*	
S(4)-S(1)-S(3)	58.12 (12)	58.76 (13)
S(4)-S(2)-S(3)	58.24 (13)	58.85 (13)
S(1)-S(3)-S(2)	58.35 (13)	59.10 (13)
S(1)-S(4)-S(2)	58.24 (13)	58.82 (13)
mean	58.24	58.88
S(4)-S(1)-S(2)	60.53 (13)	60.48 (14)
S(3)-S(1)-S(2)	60.99 (13)	60.41 (14)
S(4)-S(2)-S(1)	61.23 (13)	60.69 (14)
S(3)-S(2)-S(1)	60.66 (13)	60.50 (13)
S(1)-S(3)-S(4)	61.28 (13)	60.86 (14)
S(2)-S(3)-S(4)	60.71 (13)	60.76 (13)
S(1)-S(4)-S(3)	60.60 (13)	60.38 (14)
S(2)-S(4)-S(3)	61.05 (13)	60.39 (14)
mean	60.88	60.56
	S*-Fe-S*	
S(2)-Fe(1)-S(3)	105.2 (2)	104.7 (2)
S(2)-Fe(1)-S(4)	105.4 (2)	105.1 (2)
S(3)-Fe(1)-S(4)	103.6 (2)	104.1 (2)
S(1)-Fe(2)-S(3)	105.6 (2)	104.8 (2)
S(1)-Fe(2)-S(4)	106.1 (2)	104.9 (2)
S(3)-Fe(2)-S(4)	103.1 (2)	104.1 (2)
S(1)-Fe(3)-S(4)	105.6 (2)	105.5 (2)
S(2)-Fe(3)-S(4)	105.5 (2)	105.4 (2)
S(1)-Fe(3)-S(2)	103.8 (2)	104.5 (2)
S(1)-Fe(4)-S(3)	104.8 (2)	105.0 (2)
S(2)-Fe(4)-S(3)	104.7 (2)	104.4 (2)
S(1)-Fe(4)-S(2)	103.6 (2)	104.7 (2)
mean	104.8	104.8
	S-C(ring)	
S(5)-R(1)C(1)	1.774 (15)	1.759 (15)
S(6)-R(2)C(1)	1.764 (13)	1.737 (14)
S(7)-R(3)C(1)	1.740 (17)	1.773 (16)
S(8)-R(4)C(1)	1.784 (14)	1.735 (13)
mean	1.766 (19)	1.751 (26)

[a] If given, the figure in parentheses following a mean value is the larger of the standard deviations for an *individual* value estimated from the inverse matrix or on the assumption that the values averaged are from the same population. It is likely that the standard deviations from the inverse matrix are somewhat underestimated. The estimated standard deviation of the mean is not given for any angular quantity, as the variations exceed those expected from a sample taken from the same population.

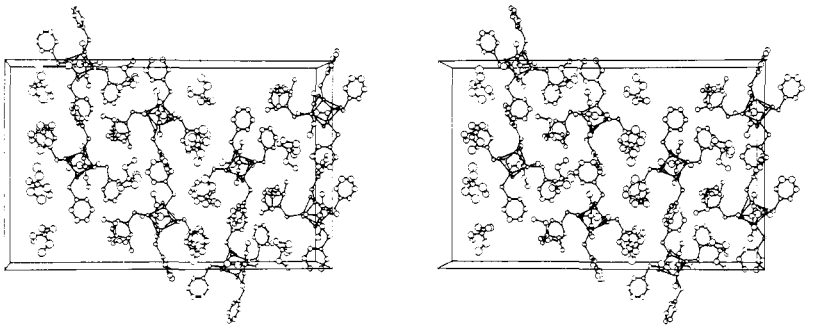

Figure 2. A stereoview of the unit cell of $(Et_3MeN)_3[Fe_4S_4(SPh)_4]$; the z axis goes from left to right, the y axis from bottom to top, and the view is down the x axis. The 15% probability level of the thermal ellipsoids is shown. Hydrogen atoms are omitted.

structures of $[Fe_4S_4(SPh)_4]^{3-}$ attention is directed to the bond angle and distance data in Table IV, atomic displacements from best weighted least-squares planes in Table V, and the principal distances, maximally congruent core and Fe_4 orientations, and the atom labeling scheme in Figure 1. (1) $[Fe_4S_4(SPh)_4]^{3-}$ exhibits a cubane-type geometry with the $[Fe_4S_4*]^+$ core structures of the two independent anions distorted from idealized T_d-$\bar{4}3m$ symmetry toward the tetragonal point group D_{2d}-$\bar{4}2m$; there is no imposed crystallographic symmetry. All structures in Figure 1 are oriented such that the idealized $\bar{4}$ axis of each passes through the top and bottom faces of the polyhedra. (2) The six diagonal planes (1-6) through the cores are nearly perfect. (3) Each Fe_2S_2* polyhedral face is a distinctly nonplanar rhomb (planes 7-12, mean S*-Fe-S* and Fe-S*-Fe angles 104.8 and 79.9°, respectively). (4) Core distances and angles under D_{2d} symmetry resolve into the sets Fe-S*, 4 long ($\parallel$ to $\bar{4}$) + 8 short ($\perp$ to $\bar{4}$); S*···S*, 2 short ($\perp$ to $\bar{4}$) + 4 long (in faces $\parallel$ to $\bar{4}$); S*-S*-S*, 4 + 8. Divisions of the following parameters into sets consistent with this symmetry are not experimentally distinct: Fe···Fe (2 + 4), Fe-Fe-Fe, S*-Fe-S*, Fe-S*-Fe (all 4 + 8). (5) The Fe_4 group is a slightly imperfect tetrahedron whereas the S_4* group is severely distorted from tetrahedral geometry; e.g., in anion 1 mean values of the two short and four long S*···S* distances are 3.592 (5) and 3.690 (4) Å, respectively. (6) From (4) and (5) the independent $[Fe_4S_4*]^+$ cores are *elongated* along the $\bar{4}$ axis. (7) The $Fe_4S_4*S_4$ clusters are devoid of symmetry as seen from the large variation of S-Fe-S* angles (98.3-123.6° in anion 1, 101.2-119.9° in anion 2); this behavior presumably arises from crystal packing effects. (8) Terminal Fe-S distances of each anion are within 3σ of one another, providing an indication not derived from core parameters of the apparent virtual equivalence of Fe sites. The mean values of 2.295 (3) and 2.294 (3) Å are 0.032 and 0.031 Å longer than the corresponding value in $[Fe_4S_4(SPh)_4]^{2-}$ (Table IX). In the $Rd_{ox,red}$ analogues $[Fe(S_2\text{-}o\text{-}xyl)_2]^{-,2-}$ [20] the Fe^{II}-S distance is 0.089 Å longer than the Fe^{III}-S distance. Thus the longer distance in $[Fe_4S_4(SPh)_4]^{3-}$ (formally 3Fe(II) + Fe(III)) vs. $[Fe_4S_4(SPh)_4]^{2-}$ (formally 2Fe(II) + 2Fe(III)) is consistent with increased Fe(II) core charzcter, and the difference in distances is close to that approximated from formal valences (0.089/4 = 0.022 Å). (9) Thermal parameters (Table II) and root mean square vibrational amplitudes (Table VII) of cluster atoms of both anions are entirely comparable with those in the more accurately determined $(Me_4N)_2[Fe_4S_4(SPh)_4]$ structure,[11] indicating little if any difference in possible disorder of cluster atom positions in the dianion and trianions. The question of disorder will be further considered in relation to Mössbauer spectral results. (10) Anions 1 and 2 do not differ in any structurally significant way.

Structural Trends in the Cubane $M_4X_4L_4$ Series and Jahn-Teller Distortions. Analogue complexes containing $Fe_4S_4*S_4$ clusters are members of the series of generalized cubane-type complexes $M_4X_4L_4$ (X = bridging ligand). The following pattern of M_4X_4 core geometries[24] emerges from examination of some 23 structures: (1) eight species[25] with closed shell M ions and nonbonding M···M distances have imposed or idealized T_d symmetry; of these two[25ab] are virtually perfect cubes (M-X/M-M = 0.71, X-M-X = M-X-M = 90°) and three[25ef] closely approach or achieve the other limiting T_d configuration formed from two concentric interpenetrating tetrahedra approaching a regular stellated tetrahedron (M-X/M-M = 0.92, X-M-X = 66°26′;[27] (2) five species[28] exhibit nonuniform core distortions and symmetries below D_{2d} which have been ascribed to intra- and intermolecular steric interactions (3) seven species with at least two bonding M···M distances assume structures consistent with the absence[29a] or presence[10-14,29b] of possible Jahn-Teller distortions. These distortions are permitted on the basis of the electronic ground states which have been predicted by the qualitative symmetry-factored MO model of Dahl and co-workers.[29a,30,31] The noncubic core structures of $HP_{red,ox}$,[3b,21] *P. aerogenes* Fd_{ox},[3,33] and $[Fe_4S_4(SR)_4]^{2-}$ have been rationalized in terms of the conflicting stereochemical demands of tetrahedral angles at Fe and bond angles $\geq$90° at S*.[3b,26] The ratios of average core distances for these species are between the limits in (1), and these demands presumably contribute to the lack of stabilization of perfect cube structures. But degradation of core symmetry from T_d to the idealized D_{2d} configuration I must arise from another source.

The original proposals[29a,34,35] that lower than T_d core symmetry in proteins and analogue dianions may occur as the consequence of first-order Jahn-Teller distortions are supported by structural behavior in the $M_4X_4L_4$ series. Recent additions to this series are $[Fe_4S_4(SCH_2CH_2CO_4)_4]^{6-}$,[12] $[Fe_4Se_4(SPh)_4]^{2-}$,[14] and $[Fe_4S_4Cl_4]^{2-}$,[13] whose $[Fe_4X_4]^{2+}$ cores, as those of other analogues and isoelectronic protein sites, conform to the same idealized symmetry. The form of distortion toward D_{2d} is *compression* along the $\bar{4}$ axis. Both the qualitative MO treatment[10b,29a] and a preliminary SCF-Xα electronic structural model[35] of $[Fe_4S_4(SR)_4]^{2-}$ in T_d symmetry admit orbitally degenerate ground states and thus first-order Jahn-Teller distortions. The latter model suggests a $^3T_1$ ground state from theconfiguration$\cdots 10t_2^4$, in which t_2 orbitals are antibonding and mainly Fe_4 in character; a $^2T_2$ state follows for $[Fe_4S_4(SR)_4]^{3-}$ inasmuch as calculations for the R = H trianion indicate that the orbital energy order is maintained.[35b] Distortion of a T_d $[Fe_4S_4]^{2+,+}$ core to the observed idealized D_{2d} geometry is allowed by one or a combination of modes of E symmetry species only,[36] thereby removing ground-state orbital degeneracy ($t_{2,2}^4 \rightarrow e^4b_{1,2}^0$). The physical situation is approximated by the representation in Figure 3, where it is shown that two phases of a component of an E mode[37] can lead to D_{2d} structures compressed or elongated along the $\bar{4}$ axis. These structures roughly correspond to the core geometries of $[Fe_4S_4(SR)_4]^{2-}$ and $[Fe_4S_4$-

Table V. Core Atom Deviations from Best Weighted Least-Squares Planes for $[Fe_4S_4(SPh)_4]^{3-}$

Atom	deviations, Å, from plane no.											
	1	2	3	4	5	6	7	8	9	10	11	12
						Anion 1						
Fe(1)		0.009 (4)		−0.010 (4)		−0.002 (4)			−0.067 (4)	0.063 (3)		0.072 (4)
Fe(2)	−0.012 (3)		0.004 (2)			0.000 (1)	0.000 (1)			0.066 (2)	0.022 (2)	
Fe(3)	0.016 (3)			0.011 (4)	0.000 (4)		−0.012 (4)	−0.098 (3)	−0.076 (4)			
Fe(4)		−0.009 (4)	−0.022 (4)		0.000 (4)			−0.086 (3)			0.025 (4)	0.082 (4)
S(1)		0.021 (6)		−0.022 (5)		−0.003 (6)	0.303 (6)	0.255 (5)			−0.287 (5)	
S(2)	−0.031 (5)		0.022 (5)			0.002 (6)		0.271 (5)	0.249 (6)			−0.239 (6)
S(3)	0.027 (5)			0.021 (5)	−0.001 (5)					−0.299 (5)	−0.274 (5)	−0.207 (6)
S(4)		−0.019 (5)	−0.036 (5)		0.001 (5)		0.288 (6)		0.220 (5)	−0.313 (5)		
						Anion 2						
Fe(1)		0.004 (3)		0.005 (4)		−0.001 (4)			−0.073 (4)	−0.093 (3)		−0.085 (4)
Fe(2)	−0.005 (4)		−0.001 (4)			0.001 (4)	0.073 (4)			−0.082 (3)	0.076 (4)	
Fe(3)	0.005 (4)			−0.005 (4)	0.002 (4)		0.078 (4)	0.085 (3)	−0.084 (4)			
Fe(4)		−0.004 (3)	0.001 (4)		−0.002 (4)			0.081 (3)			0.075 (4)	−0.076 (4)
S(1)		0.008 (5)		0.011 (6)		−0.003 (6)	−0.243 (6)	−0.269 (5)			−0.249 (6)	
S(2)	−0.011 (6)		−0.002 (5)			0.003 (6)		−0.248 (5)	0.234 (5)			0.250 (6)
S(3)	0.010 (5)			−0.010 (5)	0.003 (5)					0.231 (5)	−0.219 (5)	0.223 (6)
S(4)		−0.008 (5)	0.002 (6)		−0.004 (6)		−0.242 (6)		0.241 (6)	0.267 (5)		

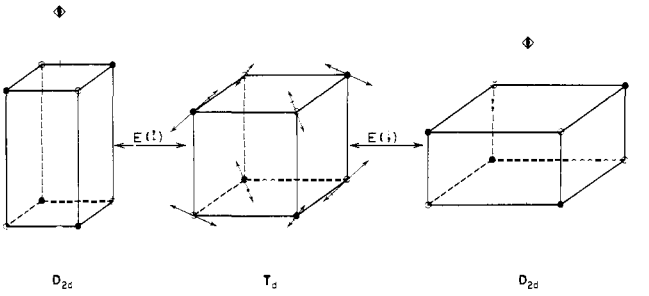

Figure 3. Schematic illustration of distortion of a T_d M_4X_4 unit to D_{2d} structures elongated or compressed along the $\bar{4}$ axis by the two phases (↑,↓) of one component of a normal vibration of E symmetry. The other component of this E mode could equally well be used in the illustration.

$(SPh)_4]^{3-}$, respectively. The structural comparison in Table IX shows that the most significant difference between dianions and this trianion is the form of the distortion toward D_{2d}, and that these distortions mainly involve changes in S_4* atomic positions relative to the slightly imperfect tetrahedral Fe_4 units of nearly constant geometry. Given the structural uniformity of five isoelectronic complexes, it appears certain that the compressed tetragonal geometry is not an artifact of crystal packing and is the true minimal energy configuration of the $[Fe_4X_4]^{2+}$ core (X = S*, Se). The essentially constant structure of the two independent $[Fe_4S_4(SPh)_4]^{3-}$ anions is suggestive of a similar designation for the elongated tetragonal geometry of $[Fe_4S_4]^{+}$ cores. However, the structure of $[Fe_4S_4(SCH_2Ph)_4]^{3-}$ in its Et_4N^+ salt departs from this geometry.[38] The 12 Fe-S* distances divide into two sets of six with mean values of 2.331 (range 2.325-2.334 Å) and 2.302 Å (range 2.296-2.308 Å), and are arranged such that the core symmetry approaches C_{2v}.

In the sections which follow physicochemical data for trianions $[Fe_4S_4(SR)_4]^{3-}$ with R = Ph and CH_2Ph are presented. Data for the two trianions are compared with each other and with corresponding information for protein sites in order to examine the sensitivity of electronic (and, inferentially, structural) properties to changes between the crystalline and solution phases, and to provide more detailed confirmatory evidence for the isoelectronic relationships between $[Fe_4S_4(SR)_4]^{3-}$ and proteins in series (1).

Electronic Absorption Spectra. Spectral data for $[Fe_4S_4(SR)_4]^{2-,3-}$ complexes are presented elsewhere.[15,19] In the present context the most important observation is that the prominent maxima of $[Fe_4S_4(SR)_4]^{2-}$ in the visible region (417 nm (R = CH_2Ph), 445 nm (R = Ph) in acetonitrile solution) are abolished in the spectra of $[Fe_4S_4(SR)_4]^{3-}$, which consist of gradually rising asorption into the ultraviolet and about a 50% decrease in intensity compared with dianions at wavelengths longer than ~420 nm. A qualitatively similar behavior is observed in Fd_{ox}/Fd_{red} spectral comparisons.[39]

EPR Spectra. When examined in frozen aqueous solutions Fd_{red} proteins containing one or two 4-Fe sites exhibit two EPR spectral characteristics presently unique among paramagnetic centers in biology: rhombic spectra centered near $g \sim 1.94$ with $g_{av} < 2$, and relaxation properties such that signals are difficulty observable above 40-50 K under the fairly typical experimental conditions of ≲1 mM protein concentrations and microwave power levels at or below the 1-20 mW range. Table X provides a comparison between g values of typical proteins[40-43] and two $[Fe_4S_4(SR)_4]^{3-}$ species. The temperature dependence of the spectra of a 0.93 mM solution of $[Fe_4S_4(SPh)_4]^{3-}$ at 4.2-104 K is presented in Figure 4; under the same experimental conditions solutions of $[Fe_4S_4(SCH_2Ph)_4]^{3-}$ afford very similar spectra. Synthetic trianion spectra are of axial symmetry having principal g values

Table VII. Root Mean Square Amplitudes of Vibration (Å)

atom	anion 1			anion 2		
	min	int	max	min	int	max
Fe(1)	0.211 (4)	0.224 (4)	0.241 (4)	0.205 (5)	0.231 (4)	0.259 (4)
Fe(2)	0.206 (4)	0.216 (4)	0.231 (4)	0.207 (5)	0.223 (4)	0.257 (4)
Fe(3)	0.216 (4)	0.231 (4)	0.247 (4)	0.218 (5)	0.227 (4)	0.262 (4)
Fe(4)	0.212 (4)	0.222 (4)	0.248 (4)	0.206 (4)	0.226 (4)	0.249 (4)
S(1)	0.215 (7)	0.242 (6)	0.254 (6)	0.229 (7)	0.244 (7)	0.264 (6)
S(2)	0.204 (8)	0.243 (6)	0.274 (6)	0.201 (8)	0.237 (7)	0.283 (6)
S(3)	0.223 (7)	0.225 (7)	0.242 (6)	0.218 (7)	0.238 (7)	0.243 (6)
S(4)	0.212 (7)	0.238 (6)	0.254 (6)	0.200 (8)	0.242 (7)	0.289 (6)
S(5)	0.214 (9)	0.266 (7)	0.319 (6)	0.223 (9)	0.279 (8)	0.352 (6)
S(6)	0.221 (8)	0.243 (7)	0.332 (6)	0.212 (9)	0.279 (7)	0.316 (6)
S(7)	0.241 (8)	0.272 (7)	0.314 (6)	0.238 (9)	0.267 (8)	0.338 (6)
S(8)	0.223 (9)	0.286 (7)	0.314 (6)	0.222 (8)	0.244 (7)	0.306 (6)

Table IX. Comparison of Mean Values of Selected Structural Parameters for $[Fe_4S_4^*(SPh)_4]^{2-}$ and $[Fe_4S_4^*(SPh)_4]^{3-}$

distance/angle[a]	$[Fe_4S_4^*(SPh)_4]^{2-}$[b]	$[Fe_4S_4^*(SPh)_4]^{3-}$	
		anion 1	anion 2
Fe-S	2.263	2.295	2.294
Fe-S*	2.267 (4), 2.296 (8)[c]	2.286 (8), 2.354 (4)[d]	2.290 (8), 2.348 (4)[d]
Fe···Fe	2.736	2.743	2.744
S*···S*	3.592 (4), 3.650 (2)[e]	3.592 (2), 3.690 (4)[f]	3.617 (2), 3.679 (4)[g]
S-Fe-S*	114.4	113.6	113.7
Fe-S*-Fe	73.5	72.9	72.9
S*-Fe-S*	104.3	104.8	104.8
Fe-Fe-Fe	59.99	59.98	60.00

[a] Number of values averaged indicated in parentheses where two distances or angles are given; otherwise, the mean of all values is given. [b] Me_4N^+ salt; data from ref 11. [c-g] Mean of all values. [c] 2.286. [d] 2.309. [e] 3.611. [f] 3.657. [g] 3.658.

Table X. EPR Data for Fd_{red} Proteins and $[Fe_4S_4(SR)_4]^{3-}$

protein/analogue	medium	g values	g_{av}	ref
Bacillus polymyxa Fd_{red}[a]	aq buffer	1.88, 1.93, 2.06	1.96	40
Bacillus stearothermophilus Fd_{red}[a]	aq buffer	1.89, 1.93, 2.07	1.96	41
Chromatium $HP_{s\text{-}red}$[a]	80% Me_2SO/H_2O	1.93, 2.04	1.97	9
Micrococcus lactyliticus Fd_{red}[b,c]	aq buffer	1.89, 1.94, 2.07	1.97	42
Clostridium pasteurianum Fd_{red}[b]	80% Me_2SO/H_2O	1.94, 2.06	1.98	43
Rhodospirillum rubrum Fd III	aq buffer	1.94, 2.03	1.97	5b
$[Fe_4S_4(SCH_2Ph)_4]^{3-}$	MeCN	1.93, 2.04	1.97	*d*
	DMF	1.93, 2.03	1.96	*d*
$[Fe_4S_4(SPh)_4]^{3-}$	MeCN	1.93, 2.06	1.97	*d*
	DMF	1.93, 2.05	1.97	*d*

[a] 4-Fe protein. [b] 8-Fe protein. [c] Partially reduced. [d] This work.

in good agreement with those from spectra of chemical and electrochemical reduction products of $[Fe_4S_4(SR)_4]^{2-}$,[16] thereby confirming prior identification of the latter as $[Fe_4S_4(SR)_4]^{3-}$. The rhombic spectra of *C. pasteurianum*[9bc,43] and other[9bc] Fd_{red} proteins in aqueous solution revert to an axial or near-axial shape, very similar to those of $[Fe_4S_4(SR)_4]^{3-}$ in aprotic solvents, when observed in 80% Me_2SO/H_2O. In this medium protein tertiary structure is unfolded. *R. rubrum* Fd III provides the only example in aqueous solution of an axial spectrum of a reduced 4-Fe protein site.[5b]

The temperature and microwave power saturation characteristics of $[Fe_4S_4(SPh)_4]^{3-}$ in a 0.46 mM acetonitrile solution are shown in Figure 5. The temperature and power (P) ranges encompass the experimental conditions used in the determination of nearly all published Fd_{red} spectra. Because signal intensity is proportional to $P^{1/2}$ in the absence of saturation, the descending portions of the plots represent regions of partial saturation. Although a comparable body of data has not been reported for reduced proteins, less extensive observations of the latter in the normal and unfolded configurations suggest similar behavior. In aqueous solutions *B. stearothermophilus* Fd_{red} is appreciably saturated at 10 K/1 mW,[41] *D. gigas* FdI_{red} at 10 K[6a] (P unspecified), and *B. polymyxa* Fd_{red} at <10 K but not at 12 K with $P = 27$ μW.[40] Cammack[9c] has described the axial spectra of unfolded proteins as being readily detectable below 35 K and readily saturated at 10 K. Examination of Figures 4 and 5 reveals that the highest practical temperature for $[Fe_4S_4(SR)_4]^{3-}$ signal observation under normal experimental conditions is ca. 60 K, and the signal intensity and resolution are mcuh enhanced below ca. 35 K. Resolved in the high-temperature spectra is a weak free-radical signal at $g = 2$, consistently observed in all isolated samples of $[Fe_4S_4(SR)_4]^{3-}$. This resonance accounts for the small line shape irregularity, absent in unfolded protein spectra, in the trough region between the axial signals.

The g-value data and temperature and microwave power dependencies of signal intensities (implying comparable electron spin relaxation times) further support designation of $[Fe_4S_4(SR)_4]^{3-}$ species as analogues of Fd_{red} sites. The enhanced analogue-Fd_{red} spectral similarities under conditions of protein unfolding are consistent with previous findings[7a,44]

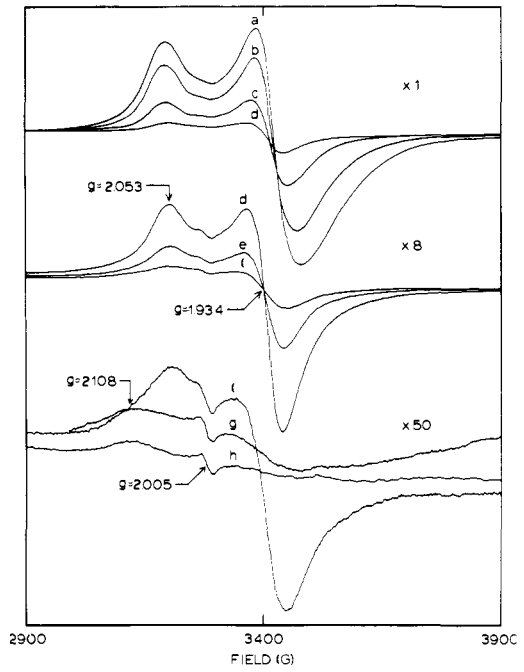

Figure 4. Temperature dependence of the EPR spectra of a 0.93 mM solution of $(Et_4N)_3[Fe_4S_4(SPh)_4]$ in DMF. Spectrometer settings: microwave power, 5 mW; frequency, 9.21 GHz; modulation amplitude, 40 G. Multiplication factors refer to total gain relative to the top spectral series: (×1) (a) 4.2, (b) 14.0, (c) 24.0, (d) 35.0 K; (×8) (d) 35.0, (e) 42.0, (f) 62.0 K; (×50) (f) 62.0, (g) 84.0, (h) 104.0 K.

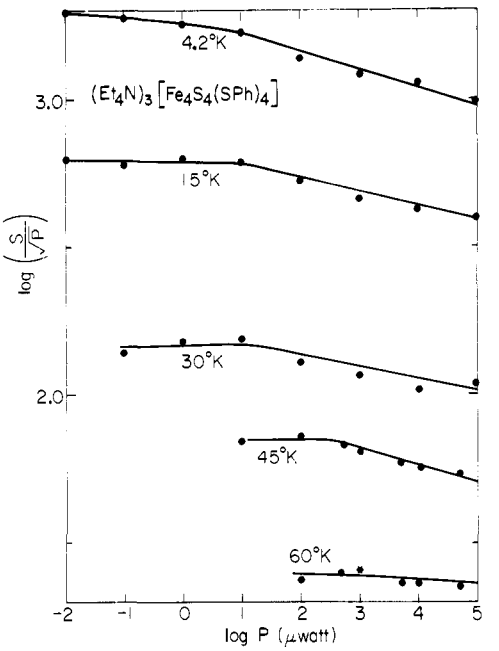

Figure 5. Temperature and microwave power dependence of integrated, normalized signal intensities S (arbitrary units) of 0.46 mM $(Et_4N)_3[Fe_4S_4(SPh)_4]$ in acetonitrile solution. Spectra were recorded at 9.21 GHz with a modulation frequency of 10^5 kHz and a modulation amplitude of 40 G.

that disruption of protein structure affords $[Fe_4S_4(S\text{-}Cys)_4]$ sites in a condition such that features inherent to isoelectronic $[Fe_4S_4(SR)_4]$ synthetic clusters are closely approached. Evidently distortions of sites from axial symmetry as observed for proteins in their native states are absent or insufficiently large to be detectable in the EPR spectra of $[Fe_4S_4(SR)_4]^{3-}$ clusters in frozen solutions.

Mössbauer Spectra. A. Polycrystalline Solids. Spectra of various $[Fe_4S_4(SR)_4]^{2-}$ species consist of one symmetric quadrupole doublet down to temperatures as low as 1.5 K.[17,45] These and other spectroscopic results,[45] together with structural data[10b-12] (Figure 1), establish the equivlanece of the four Fe sites in analogue dianions. By Mössbauer spectral criteria this situation is closely approached in a number of Fd_{ox} proteins,[46,47] including the 4-Fe Fd_{ox} from *B. stearothermophilus*.[41,47,48] Representative spectra of polycrystalline Et_4N^+ salts of $[Fe_4S_4(SPh)_4]^{3-}$ and $[Fe_4S_4(SCH_2Ph)_4]^{3-}$ at various temperatures in zero applied magnetic field are shown in Figures 6-8. These contrast sharply with those of the corresponding dianions. The spectra of the two trianions, briefly reported earlier,[18] are distinctly different but share the feature that both can be characterized as resulting from the superposition of at least two quadrupole doublets with temperature variable quadrupole splittings and line widths.

Least-squares fits of Lorentzian line shapes[49] to the experimental spectra, assuming two distinguishable subsites in $[Fe_4S_4(SR)_4]^{3-}$, have led to the derived values of spectral parameters for the pairs of quadrupole doublets presented in Table XI. If line widths and intensities are allowed to vary unconstrained, spectra of $[Fe_4S_4(SPh)_4]^{3-}$ yield a relative integrated intensity ratio for the two subsites of close to 1:1 while for $[Fe_4S_4(SCH_2Ph)_4]^{3-}$ ratios in the 1:1 to 2:1 range are obtained. The same relative intensities are produced if the line widths and areas under the absorption features associated with the same subsite are constrained to be equal. However, satisfactory fits for $[Fe_4S_4(SCH_2Ph)_4]^{3-}$ are also obtained by imposing the constraint of equal integrated intensities for the

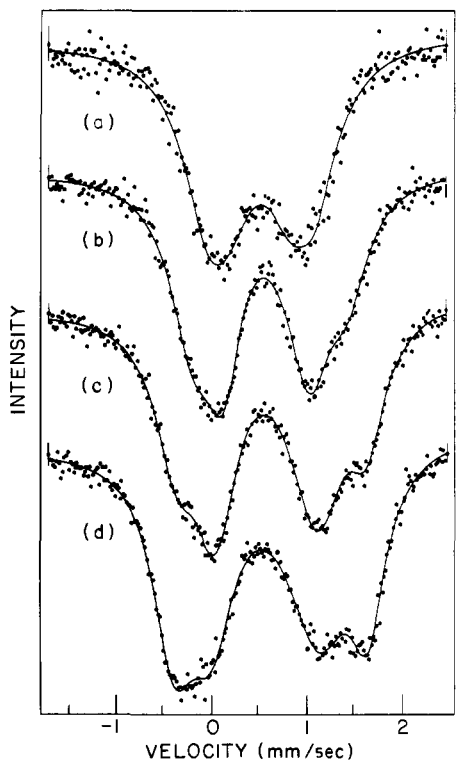

Figure 6. Mössbauer spectra of polycrystalline $(Et_4N)_3[Fe_4S_4(SPh)_4]$ at 200 (a), 77 (b), 25 (c), and 4.2 K (d). The $^{57}Co/Rh$ source is at room temperature. Solid lines are least-squares fits to the data assuming two Fe subsites per 4-Fe cluster.

two subsites. Owing to the unresolved nature of the spectra of this trianion even at the lowest temperature, the relative intensities of its two Fe subsites cannot be further defined from fits to zero-field spectra alone.

The suitability of $[Fe_4S_4(SR)_4]^{3-}$ complexes as Fd_{red} site analogues is further emphasized by spectral comparison with

Table XI. Mössbauer Data for $[Fe_4S_4(SR)_4]^{3-}$ and a Fd_{red} Protein

compd	T, K	$\delta^{b,c}$	$\Delta E_Q{}^b$	$\Gamma^{b,d}$	A^e
$(Et_4N)_3[Fe_4S_4(SPh)_4]^a$	4.2	0.64 ± 0.02[f]	2.04 ± 0.03[f]	0.52	0.43 ± 0.05[f]
		0.57	1.13	0.65	0.57
	25	0.63	2.00	0.50	0.43
		0.57	1.07	0.62	0.57
	77	0.61	1.63	0.53	0.44
		0.56	0.90	0.60	0.56
	200	0.53	0.89	0.70	
(in CH_3CN solution)	4.2	0.63	2.01	0.53	0.44
		0.57	1.11	0.64	0.56
$(Et_3MeN)_3[Fe_4S_4(SPh)_4]^a$	4.2	0.62	1.98	0.55	0.45
		0.58	1.10	0.67	0.55
$(Et_4N)_3[Fe_4S_4(SCH_2Ph)_4]^a$	4.2	0.60	1.41	0.44	0.40
		0.60	0.93	0.52	0.60
	20	0.62	1.45	0.42	0.35
		0.60	0.94	0.45	0.65
	82	0.61	1.07	0.42	0.48
		0.56	0.89	0.45	0.52
	184	0.52	0.88	0.48	
(in CH_3CN solution)	4.2	0.64	2.01	0.53	0.42
		0.59	1.12	0.63	0.58
B. stearothermophilus Fd_{red}[g]	4.2	0.58	1.89		
		0.50	1.32		
	77	0.59	1.84	0.36	
		0.49	1.20	0.36	

[a] Crystalline sample. [b] mm/s. [c] Referenced to metallic iron at room temperature. [d] Line width parameter. [e] Relative area assuming two quadrupole doublets in an unconstrained computer fit. [f] Estimated uncertainty for the indicated quantity from computer spectral fitting. [g] Reference 48.

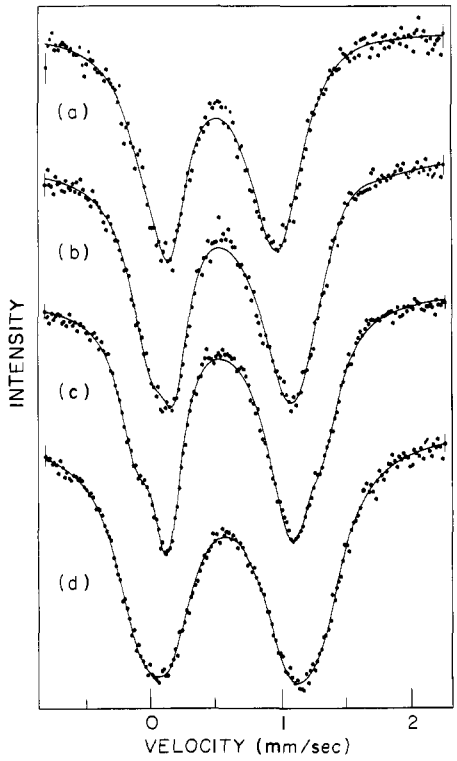

Figure 7. Mössbauer spectra of polycrystalline $(Et_4N)_3[Fe_4S_4(SCH_2Ph)_4]$ at 184 (a), 82 (b), 20 (c), and 4.2 K (d). The $^{57}Co/Rh$ source is at room temperature. Solid lines are least-squares fits to the data assuming two Fe subsites per 4-Fe cluster.

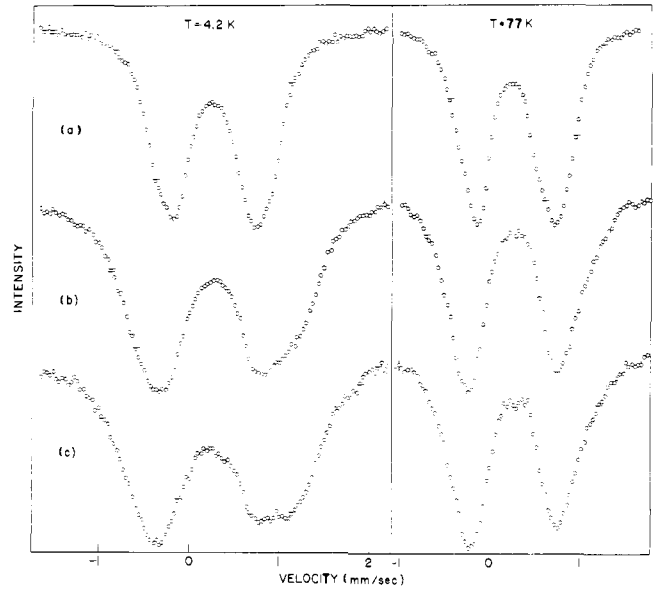

Figure 8. Mössbauer spectra at 4.2 and 77 K: (a) polycrystalline $(Et_4N)_3[Fe_4S_4(SCH_2Ph)_4]$; (b) ~30 mM $(Et_4N)_3[Fe_4S_4(SCH_2Ph)_4]$ in acetonitrile solution; (c) ~30 mM $(Et_4N)_3[Fe_4S_4(SPh)_4]$ in acetonitrile solution.

B. stearothermophilus Fd_{red},[41] the only single-site 4-Fe protein which has been thoroughly studied by Mössbauer spectroscopy.[47,48] This protein also exhibits two overlapping quadrupole doublets of about equal intensity whose parameters (Table XI) are decidedly similar to those of the trianions. Hence, Fe subsite inequivalence on the Mössbauer time scale (detectable lifetimes τ of $\gtrsim 10^{-7}$ s) is a property intrinsic to $[Fe_4S_4(SR)_4]^{3-}$ clusters in the solid and solution states and is not necessarily a consequence of protein structural effects.

The availability of isomer shift (δ) data for $[Fe_4S_4(SR)_4]^{3-}$ species now permits significant examination of the dependence of δ on the mean *formal* oxidation state of Fe, which is unambiguously defined by the net charge of each analogue complex. The assembly of isomer shift data[17,20,46,47,50-54] in Table XII augments other tabulations for proteins only[46,47] and fully substantiates the mean formal oxidation state designations given for the latter. The monotonic displacement of δ values to increasingly positive velocities with decreasing

Table XII. Variation of Isomer Shifts of Active Site Analogues and Proteins with Formal Oxidation State of Iron

mean formal oxidation state	analogue	δ^a	protein	δ^a	ref
+3	$[Fe(S_2\text{-}o\text{-}xyl)_2]^-$	0.13	Rd_{ox}	0.25	20, 47, 50
	$[Fe_2S_2(S_2\text{-}o\text{-}xyl)_2]^{2-}$	0.17	2-Fe Fd_{ox}[d]	0.26	47. 51
+2.75	*b*		HP_{ox}[e]	0.31	47, 52
+2.50	$[Fe_4S_4(SPh)_4]^{2-}$	0.35	8-Fe Fd_{ox}[f]	0.43	17, 46, 47
	$[Fe_4S_4(SCH_2Ph)_4]^{2-}$	0.34	4-Fe Fd_{ox}[g]	0.42	17, 41
			HP_{red}[e]	0.42	47, 52
+2.25	$[Fe_4S_4(SPh)_4]^{3-}$	0.56, 0.61[c]	$HP_{s\text{-}red}$[e]	0.59	47, 53
	$[Fe_4S_4(SCH_2Ph)_4]^{3-}$	0.56, 0.61[c]	8-Fe Fd_{red}[f]	0.57	46, 47
			4-Fe Fd_{red}[g]	0.49, 0.59	*c*
+2	$[Fe(S_2\text{-}o\text{-}xyl)_2]^{2-}$	0.61	Rd_{red}	0.65	20, 47, 50
	$[Fe(SPh)_4]^{2-}$	0.64			54
	b		2-Fe Fd_{red}[d]	0.60[h]	47

[a] 77 K, mm/s relative to metallic iron. [b] Not yet isolated. [c] Table XI. [d] From spinach. [e] From *Chromatium*. [f] From *C. pasteurianum*. [g] From *B. Stearothermophilus*. [h] Fe(II) site.

oxidation state is consistent with simple theoretical considerations and also has been observed for various Fe-S phases containing integral and fractional metal oxidation states.[55]

The nature of the inequivalent sites in $[Fe_4S_4(SR)_4]^{3-}$ has been examined with the aid of magnetically perturbed spectra. Application of external fields H_0 induces magnetic hyperfine structure in the spectra of R = CH_2Ph and Ph complexes[18] shown in Figure 9. At $H_0 \lesssim 40$ kOe broadened unresolved spectra are obtained but at $40 \leq H_0 \leq 80$ kOe two pairs of lines are observed which flank a central unresolved absorption area. With increasing H_0 the splitting of one pair of lines decreases while the splitting of the other pair increases, consistent with the existence of at least two magnetically inequivalent sites and antiparallel spin coupling within the $[Fe_4S_4]^+$ core. The overall magnitudes of the splittings are about 50% smaller in $[Fe_4S_4(SCH_2Ph)_4]^{3-}$ than in $[Fe_4S_4(SPh)_4]^{3-}$. In both cases the magnetic fields observed at the Fe nuclei are different from the applied fields, indicating the presence of magnetic hyperfine structure arising from unpaired s-electron spin density at the Fe sites. Moreover, the magnetic hyperfine interaction constants estimated from the observed splittings are different for the two ttw magnetic subsites, implying different spin densities at these sites.[56] Theoretical fits of the high magnetic field spectral data to obtain more exact values of the magnetic hyperfine interaction constants and relative integrated intensities of the magnetic subsites will be reported fully elsewhere.[57] The present zero-field and magnetically perturbed Mössbauer spectral characteristics are, however, sufficient to establish a clear electronic similarity between $[Fe_4S_4(SR)_4]^{3-}$ and the active site of *B. stearothermophilus* Fd_{red} in the native state. Consequently, the model II proposed originally by Dickson et

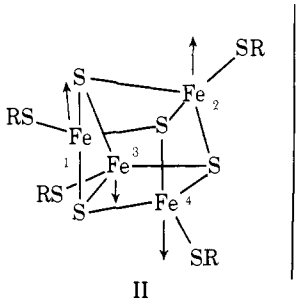

II

al.[58] for protein ground state properties and consistent with detailed spectral analysis[47,48] appears to us as an acceptable qualitative description. In Fd_{ox} sites and $[Fe_4S_4(SR)_4]^{2-}$, Fe atoms are antiferromagnetically coupled in pairs (1,2; 3,4) with

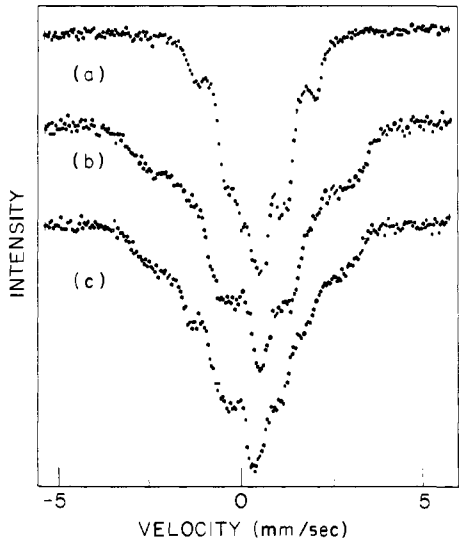

Figure 9. Mössbauer spectra at 4.2 K in a longitudinally applied magnetic field of 80 kOe: (a) polycrystalline $(Et_4N)_3[Fe_4S_4(SCH_2Ph)_4]$; (b) ~30 mM $(Et_4N)_3[Fe_4S_4(SCH_2Ph)_4]$ in acetonitrile solution; (c) ~30 mM $(Et_4N)_3[Fe_4S_4(SPh)_4]$ in acetonitrile solution.

fast electron hopping between pairs ($\tau^{-1} \gtrsim 10^7\ s^{-1}$), leading to equivalent Fe atoms of average oxidation state +2.5 (consistent with isomer shift trends, Table XII) and the observed $S = 0$ ground state (vide infra). Reduction to Fd_{red} and $[Fe_4S_4(SR)_4]^{3-}$ results in localization of the added electron on one pair ($2Fe^{2+}$), persistence of rapid hopping within the other pair, and slow transfer of electrons between pairs ($\tau^{-1} \lesssim 10^7\ s^{-1}$).[59] These pairs constitute the two Mössbauer-distinguishable sites. Based on parameters of Fd_{ox} and $[Fe_4S_4(SR)_4]^{2-}$ spectra, the more ferric-like pair is presumably associated with the doublet having the smaller isomer shift and quadrupole splitting.

B. Frozen Solutions. Differences in the zero field spectra of the Et_4N^+ salts of $[Fe_4S_4(SPh)_4]^{3-}$ and $[Fe_4S_4(SCH_2Ph)_4]^{3-}$ (Figures 6 and 7) perhaps arise from small structural variations between the two trianions. Note that the spectral parameters of $(Et_3MeN)_3[Fe_4S_4(SPh)_4]$ (Table XI), the salt on which the x-ray structure determination was performed, are indistinguishable from those of the Et_4N^+ salt. In an attempt to ascertain if the structural differences persist in the solution state, Mössbauer spectra of the two Et_4N^+ salts were recorded in frozen acetonitrile solutions. From the zero-field spectra of Figures 6 and 8 it is apparent that for $[Fe_4S_4(SPh)_4]^{3-}$ frozen solution spectra are very similar to those obtained with the

polycrystalline absorber,[60] and we conclude that this cluster has essentially the same structure in the frozen solution as in the polycrystalline solid. For $[Fe_4S_4(SCH_2Ph)_4]^{3-}$, however, spectra in the two phases (Figures 7 and 8) are dissimilar. In fact, *the frozen solution spectra of $[Fe_4S_4(SCH_2Ph)_4]^{3-}$ are very similar to the polycrystalline and frozen solution spectra of $[Fe_4S_4(SPh)_4]^{3-}$*. This important observation is borne out by comparison of spectral parameters at 4.2 K in Table XI and is further supported by the comparison of the spectra obtained at 80 kOe and 4.2 K (Figure 9). Thus we conclude that $[Fe_4S_4(SCH_2Ph)_4]^{3-}$ in acetonitrile solution has a configuration such that its Fe atoms are virtually indistinguishable from those in $[Fe_4S_4(SPh)_4]^{3-}$.

The foregoing results are also consistent with earlier Mössbauer data for $[Fe_4S_4(SCH_2Ph)_4]^{3-}$, generated by chemical reduction of the dianion in DMF/THF.[16,17] In those spectra the full magnetic hyperfine splitting was observed at $H_0 \sim 1$ kOe and 4.2 K whose magnitude is consistent with the present observation of splittings in polycrystalline and solution absorbers of $[Fe_4S_4(SPh)_4]^{3-}$ and the solution absorber of $[Fe_4S_4(SCH_2Ph)_4]^{3-}$. Differences are observed in low magnetic field spectra ($H_0 \leq 40$ kOe), which may be ascribed to electron relaxation effects. As noted earlier[18] the line width of polycrystalline $[Fe_4S_4(SPh)_4]^{3-}$ is broad, suggesting slow relaxation effects. Line widths of this trianion in frozen solutions at $H_0 = 0$ are not appreciably broader, however, and a greater magnetic hyperfine splitting is observed in small fields ($H \sim 5$ kOe) than for the polycrystalline absorber. Measurements in more dilute (<30 mM) frozen acetonitrile solutions of the two trianions confirm the trend. Thus we may characterize $[Fe_4S_4(SPh)_4]^{3-}$ and $[Fe_4S_4(SCH_2Ph)_4]^{3-}$ in both frozen acetonitrile and DMF/THF solutions as having a cluster stereochemistry approaching equivalence with that of crystalline $[Fe_4S_4(SPh)_4]^{3-}$, and electronic relaxation rates which are solvent and concentration dependent. Further support of the former point follows from magnetic susceptibility results (vide infra).

C. Temperature Dependence. At the higher temperatures the two quadrupole doublets of $[Fe_4S_4(SPh)_4]^{3-}$ and $[Fe_4S_4(SCH_2Ph)_4]^{3-}$ become less clearly resolved (Figures 6 and 7). At $T > 100$ K only one broadened quadrupole doublet is observed in each case. Thus the subsite inequivalence which is pronounced at low temperatures appears to diminish with increasing temperature such that near ambient temperature the subsites approach equivalence. Two possible causes of the temperature-dependent spectral changes are (1) retention of subsite inequivalence masked by inherent temperature dependencies of individual doublets such that the spectra at higher temperatures appear more symmetrical than is the actual structure; (2) loss of subsite inequivalence by increasingly rapid electron hopping between pairs (model (II)) or among all Fe atoms resulting in, formally, 4 $Fe^{+2.25}$ in the fast exchange limit ($\tau^{-1} > 10^7$ s^{-1}).[61] In the latter case true equivalence is possibly not reached because line widths at the highest temperatures of observation are substantially braoder[62] than those in the site-equivalent $[Fe_4S_4(SR)_4]^{2-}$ species (Γ = 0.23 mm/s at room temperature).[17,45] No decision can be made between these two cases, neither of which is necessarily inconsistent with the apparent virtual equivalence of Fe sites observed in the structures of anions 1 and 2 of $[Fe_4S_4(SPh)_4]^{3-}$ at room temperature. Structural feature (9) supports the lack of any orientational disorder of the elongated clusters in the crystal, but does not eliminate a form of "electronic" disorder in which diffraction from an instantaneous Fe^{2+} or $Fe^{2.5+}$ site (e.g., as in model II) is manifested as that from an electronically averaged $Fe^{2.25+}$ site. As illustrated by the recent study of a $[(H_3N)_5Ru(pyrazine)Ru(NH_3)_5]^{5+}$ salt,[63a] this problem is endemic to structure determinations of formal mixed valence compounds whose metal coordination sites are expected to exhibit only small dimensional differences in the limit of trapped oxidation states.[63b]

Table XIII. Magnetic Data for $[Fe_4S_4(SR)_4]^{2-,3-}$ Complexes at Selected Temperatures

	$(Et_4N)_2[Fe_4S_4(SCH_2Ph)_4]$[a]		$(Et_4N)_2[Fe_4S_4(SPh)_4]$[b]	
T, K	$\chi_t \times 10^5$[g]	μ_t, μ_B[h]	$\chi_t \times 10^5$[g]	μ_t, μ_B[h]
50.2	40.5	0.40	44.0	0.42
75.2	47.0	0.53	48.5	0.54
100.2	63.8	0.72	63.1	0.71
120.3	79.9	0.88	80.8	0.88
140.3	98.6	1.05	101	1.06
160.4	114	1.21	118	1.23
180.4	132	1.38	136	1.40
200.4	146	1.53	152	1.56
240.3	167	1.79	174	1.83
279.5	182	2.02	190	2.06
299.1	190	2.13	196	2.17
338.1	199	2.32	210	2.38
	$(Et_4N)_3[Fe_4S_4(SCH_2Ph)_4]$[c]		$(Et_4N)_3[Fe_4S_4(SPh)_4]$[d]	
T, K	$\chi_t \times 10^3$[g]	μ_t, μ_B[h]	$\chi_t \times 10^3$[g]	μ_t, μ_B[h]
4.2	335	3.35	125	2.05
10.5	141	3.44	57.4	2.19
29.4	50.1	3.44	25.8	2.46
50.2	30.6	3.50	17.4	2.64
75.2	23.0	3.72	13.5	2.85
100.2	19.2	3.92	11.5	3.03
130.3	16.5	4.14	10.3	3.27
150.4	15.0	4.26	9.78	3.43
180.4	13.7	4.44	9.07	3.62
200.4	12.9	4.55	8.70	3.73
240.3	11.8	4.76	8.28	3.99
279.5	11.2	5.00	7.94	4.21
299.1	11.0	5.13	7.89	4.35
338.1	10.3	5.28	7.63	4.54
	$(n\text{-}Pr_4N)_3[Fe_4S_4(SCH_2Ph)_4]$[e]		$(Et_3MeN)_3[Fe_4S_4(SPh)_4]$[f]	
T, K	$\chi_t \times 10^3$[g]	μ_t, μ_B[h]	$\chi_t \times 10^3$[g]	μ_t, μ_B[h]
4.2	201	2.60	123	2.03
10.6	90.5	2.77	57.7	2.21
29.8	35.6	2.91	30.4	2.69
50.4	22.6	3.02	21.0	2.91
75.2	16.8	3.18	16.8	3.18
100.2	13.6	3.31	14.2	3.37
130.2	11.9	3.52	12.3	3.58
150.3	11.1	3.65	11.5	3.71
179.9	10.3	3.85	10.5	3.89
200.3	9.90	3.98	10.2	4.04
240.1	9.37	4.24	9.19	4.20
278.6	8.87	4.45	8.81	4.43
298.9	8.68	4.56	8.69	4.56
337.3	8.44	4.77	8.33	4.74

[a-f] Diamagnetic corrections (cgsu/mol × 10^6). [a] −686. [b] −638. [c] −797. [d] −750. [e] −939. [f] −714. [g] Per 4 Fe atoms of tetrameric (t) unit, corrected for diamagnetism and impurity paramagnetism (dianions only). [h] $\mu_t = 2.828\ (\chi_t T)^{1/2}$; $\mu_{Fe} = \mu_t/2$.

Magnetic Properties. A. $[Fe_4S_4(SR)_4]^{2-}$. Results for R = CH_2Ph and Ph salts presented in Table XIII and Figure 10 reveal the general form of magnetic behavior for this oxidation level. Susceptibilities and magnetic moments per tetrameric unit are given in these and subsequent cases. Owing to the presence of appreciable paramagnetic contaminants, measured $\chi_g(T)$ curves for all preparations displayed minima near 50–60 K. Impurity corrections were made by fitting data at $T \leq T(\chi_{g,min})$ to the equation $\chi_{impurity} = C/T + A$ where C/T was used as an impurity correction and A was used to estimate the apparent temperature-independent paramagnetism ((Et4-

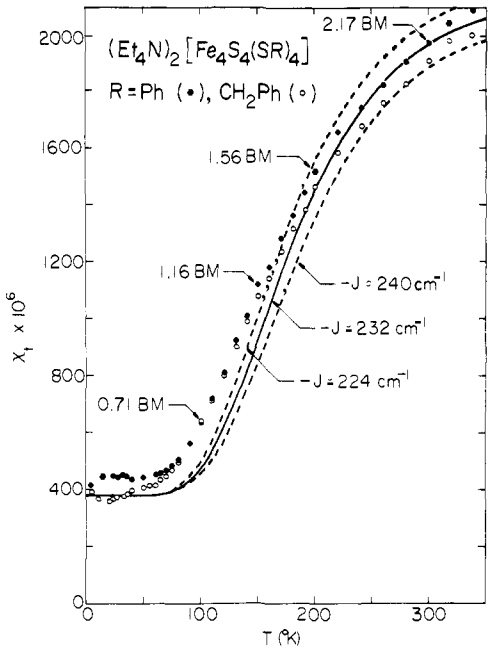

Figure 10. Temperature dependence of the magnetic susceptibility of polycrystalline Et_4N^+ salts of $[Fe_4S_4(SPh)_4]^{2-}$ (●) and $[Fe_4S_4(SCH_2Ph)_4]^{2-}$ (○). The solid line represents the best fit of the data for $(Et_4N)_2[Fe_4S_4(SCH_2Ph)_4]$ to eq A-4 in the Appendix.[22] Dashed lines indicate the theoretical behavior of this model for the indicated J values.

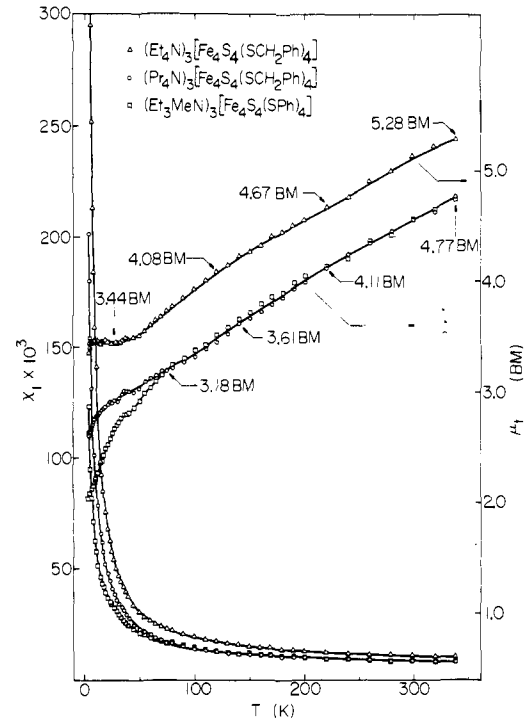

Figure 11. Temperature dependence of the magnetic susceptibilities and magnetic moments of polycrystalline $(Et_4N)_3[Fe_4S_4(SCH_2Ph)_4]$ (△), $(n\text{-}Pr_4N)_3[Fe_4S_4(SCH_2Ph)_4]$ (○), and $(Et_3MeN)_3[Fe_4S_4(SPh)_4]$ (□).

$N)_2[Fe_4S_4(SPh)_4]$, 440 × 10^{-6} cgsu, $(Et_4N)_2[Fe_4S_4(SCH_2Ph)_4]$, 380 × 10^{-6} cgsu). Plotted in Figure 10 are the final data together with theoretical $\chi_t(T)$ curves generated from an antiferromagnetic spin-coupling model[64] extended to clusters with $2Fe^{2+} + 2Fe^{3+}$ (Appendix,[22] eq A-4). The best fits for $[Fe_4S_4(SCH_2Ph)_4]^{2-}$ and $[Fe_4S_4(SPh)_4]^{2-}$, assuming $g = 2.0$, were obtained with $J = -232$ cm^{-1}. Theoretical curves and best fits are included here only to demonstrate that the experimental curves are qualitatively consistent with an antiferromagnetic type of interaction in the $[Fe_4S_4]^{2+}$ cores ($S' = 0$ ground state) as has been found with HP_{red}. For this protein Antanaitis and Moss[65] have estimated $-J \lesssim 200$ cm^{-1}, in reasonable agreement with the present results. Similar measurements by Cerdonio et al.[66] in the 20-150 K range match very closely the data above 100 K obtained here. The same model yields very similar J values for related complexes (-226 cm^{-1} for $[Fe_4Se_4(SPh)_4]^{2-}$,[14] -220 cm^{-1} for $[Fe_4S_4Cl_4]^{2-}$ [67]). In no case is a fit based on a *single* J value satisfactory over the entire temperature interval of measurement; elaboration of the model to obtain better agreement with experimental χ_t results is in progress.

B. $[Fe_4S_4(SR)_4]^{3-}$. Whereas dianion salts exhibit solid state magnetic properties which are not strongly dependent upon either cation or R substituent, this is not the case for trianion salts. Large variations in properties are observed between apparently similar species. The results in Table XIII, withdrawn from a larger data set, together with those given in graphical form in Figures 11 and 12, encompass the limiting behavior of R = Ph and CH_2Ph salts in the solid state. No corrections for paramagnetic impurities were made in any case.[68]

The general forms of the $\chi_t(T)$ curves for the polycrystalline Et_4N^+ and Et_3MeN^+ salts of $[Fe_4S_4(SPh)_4]^{3-}$ are such as to indicate net antiferromagnetic spin coupling within the clusters and a $S' = \frac{1}{2}$ ground state. Note the deviation of these curves from that for a simple $S = \frac{1}{2}$ Curie paramagnet (Figure 12). Moments at 4.2 K are 2.05 and 2.03 μ_B and increase to 4.54 and 4.74 μ_B at 338 K for the Et_4N^+ and Et_3MeN^+ salts, respectively. A value of $\mu_t = 1.71$ μ_B is calculated for the doublet ground state from the g values in Table X, indicating population of higher spin states at 4.2 K. The magnetic behavior of polycrystalline Et_4N^+ and $n\text{-}Pr_4N^+$ salts of $[Fe_4S_4(SCH_2Ph)_4]^{3-}$, shown in Figure 11, dramatizes the sensitivity of magnetic properties to the combined effects of

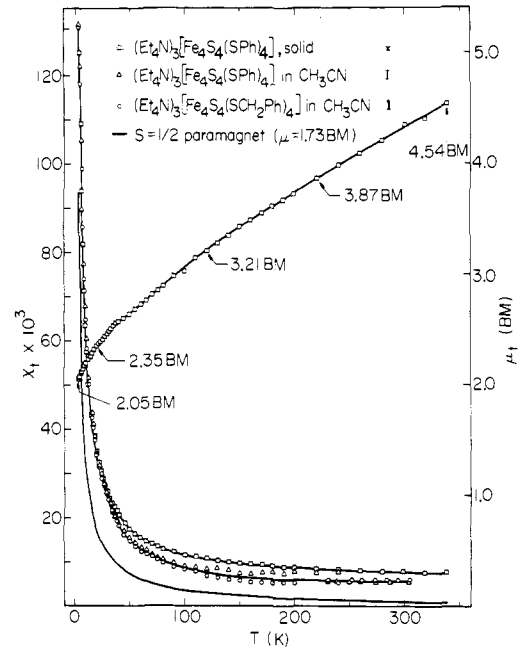

Figure 12. Temperature dependence of the magnetic susceptibilities of $(Et_4N)_3[Fe_4S_4(SPh)_4]$, polycrystalline (□) and in acetonitrile solution (△), and $(Et_4N)_3[Fe_4S_4(SCH_2Ph)_4]$ in acetonitrile solution (○). Also shown are error bars for these determinations (top), a Curie law $\chi_M(T)$ plot for an $S = \frac{1}{2}$ system (1.73 μ_B), and a plot of μ_t vs. T for polycrystalline $(Et_4N)_3[Fe_4S_4(SPh)_4]$. The smooth curve drawn near solution data points above ~100 K is meant only as a guide to the location of these points.

Table XIV. Comparison of Protein and Analogue Magnetic Properties Near Room Temperature

species	state	T, K (range)	μ_t, μ_B	ref
B. polymyxa Fd_{red}	aq soln	276-295	3.4-3.2	70
D. gigas Fd I_{red}	aq soln	278-303	4.0	6b
Fd I_{red}	aq soln	278-303	3.8	6b
$[Fe_4S_4(SPh)_4]^{3-}$	solid[a]	299	4.56	c
	CH_3CN soln	287	3.59[d]	69
$[Fe_4S_4(SCH_2Ph)_4]^{3-}$	solid[b]	299	5.13	c
	CH_3CN soln	294	3.72[e]	69

[a] Et_3MeN^+ salt. [b] Et_4N^+ salt. [c] This work. [d,e] Range of values (230-304 K). [d] 3.22-3.70 μ_B. [e] 3.30-3.77 μ_B.

cation and R group changes. Thus results for this Et_4N^+ salt differ remarkably from those for $(Et_4N)_3[Fe_4S_4(SPh)_4]$ (Figure 12). Not only does this compound show a consistently higher magnetic moment at all temperatures, but it appears to have a nearly constant moment of 3.44 μ_B below ~35 K. Additional measurements at 1.45-4.2 K show this to be a plateau region as μ_t drops to 3.06 μ_B at 1.45 K, a much larger value than found with either $[Fe_4S_4(SPh)_4]^{3-}$ salt at 4.2 K.

Magnetic results for all salts of the two $[Fe_4S_4(SR)_4]^{3-}$ trianions are consistent with an $S' = 1/2$ ground state and thermal population of $S' > 1/2$ components of a spin manifold at the lowest temperatures of measurement. The energy spacings of these higher spin states appear to be extremely sensitive to molecular distortions. Attempted fits of $\chi_t(T)$ data to an extension of the antiferromagnetic spin coupling model for a cluster with $3Fe^{2+} + Fe^{3+}$ localized sites and one J value (Appendix,[22] eq A-5) are unconvincing. Work on this problem, including additional measurements at high magnetic fields and low temperatures, is continuing. In the present context the most important observation is the large solid state magnetic difference between the two structurally defined salts $(Et_3MeN)_3[Fe_4S_4(SPh)_4]$ and $(Et_4N)_3[Fe_4S_4(SCH_2Ph)_4]$.

Magnetic measurements have been performed on frozen (4.2-200 K) and fluid[69] (230-304 K) solutions of Et_4N^+ salts of $[Fe_4S_4(SPh)_4]^{3-}$ and $[Fe_4S_4(SCH_2Ph)_4]^{3-}$ in acetonitrile. Results are plotted in Figure 11, from which it is seen that solution $\chi_t(T)$ data for both trianions closely track the values of polycrystalline $(Et_4N)_3[Fe_4S_4(SPh)_4]$ and $(Et_3MeN)_3[Fe_4S_4(SPh)_4]$ (Figure 12). As an example the moment at 4.2 K for $[Fe_4S_4(SCH_2Ph)_4]^{3-}$ in its polycrystalline Et_4N^+ salt drops from 3.35 to 2.09 μ_B in acetonitrile. Within experimental error the magnetic behaviors of $[Fe_4S_4(SPh)_4]^{3-}$ and $[Fe_4S_4(SCH_2Ph)_4]^{3-}$ in frozen and fluid acetonitrile solutions are the same over corresponding temperature intervals. Set out in Table XIV is a comparison of trianion and protein[6b,70] magnetic data near room temperature where Fd_{red} results are available. These data imply a fundamentally similar type of magnetic behavior and a closer approach to protein moments by dissolved rather than crystalline clusters. Together with the Mössbauer spectral observations the magnetic data provide convincing evidence that in frozen solution $[Fe_4S_4(SCH_2Ph)_4]^{3-}$ possesses a core structure closely approaching that of $[Fe_4S_4(SPh)_4]^{3-}$ (Figure 1). Because we consider it likely that a structure in frozen solution is less subject to perturbing environmental factors than in the crystalline state, we conclude that *an elongated tetragonal geometry is the intrinsically stable core structure of* $[Fe_4S_4(SR)_4]^{3-}$.

Cluster Structure and Redox Properties. The results of this investigation definitively establish the protein-trianion isoelectronic relationship in series (1). Having previously demonstrated the indicated relationship for dianions,[7] it is of interest to examine analogue structural changes in the light of their possible relation to the *reduction* reactions of Fd_{ox} and HP_{red} proteins. As has been shown, the unconstrained $[Fe_4S_4]^+$ core in $[Fe_4S_4(SR)_4]^{3-}$ is related to the $[Fe_4S_4]^{2+}$ core in $[Fe_4S_4(SR)_4]^{2-}$ by an elongation along the $\bar{4}$ axis, possibly corresponding to a Jahn-Teller active vibrational mode of E symmetry. It has also been established that the $[Fe_4S_4]^{2+}$ core structure in the crystalline state[10-13] is insensitive to cation and terminal ligand variations and, at the present stage of protein structure refinement, is insignificantly different from the core units of isoelectronic protein sites.

Much interest has attended the possible causes of the different one-electron reduction tendencies of the isoelectronic 4-Fe sites in Fd_{ox} and HP_{red} proteins.[2,3,71,72] Whereas the Fd_{ox}/Fd_{red} reaction (E_0' typically near -0.42 V[73]) is readily effected chemically in aqueous solution,[74] HP_{red} is reducible in an unfolded condition in 70-80% Me_2SO/H_2O solution but not in its native (aqueous) configuration.[9a] It has been proposed recently that vibronically coupled electron tunneling theory is a possible model for biological electron transfer.[75] On the basis of evidence presented here we suggest that one reason the Fd_{ox}/Fd_{red} couple operates is because protein structure at all levels allows the dimensional changes in the Fe_4S_4 core which are related to the normal vibrations of the core. In terms of the schematic representation of Figure 3 the T_d core structure is viewed as a transition state for electron transfer, which in the reducing direction requires axial expansion of the core by ca. 0.08 Å relative to the oxidized configuration. In the native form of the HP_{red} protein molecular structural forces may provide a sufficient energy barrier to this anisotropic core dimensional change that the $HP_{red}/HP_{s\text{-}red}$ potential is shifted below that for hydrogen evolution. In 80% Me_2SO/H_2O Cammack[9a] has estimated that this potential is ≤ -0.64 V, which is in the range found for Fd_{ox}/Fd_{red} and certain $[Fe_4S_4(SR)_4]^{2-,3-}$ potentials in the same medium.[44b] These results indicate that removal of protein constraints affords equivalent reducible behavior at comparable potentials. Finally, if this suggestion is correct, protein structural constraints are doubtless only one of several key factors which differentiate the reductive behavior of Fd_{red} and HP_{red}. Among these, environmental effects, specifically the larger extent of peptide-cluster hydrogen bonding[71] and greater accessibility of the redox sites to water molecules[76] for Fd_{ox} over HP_{red}, tend to favor energetically the generation of a more negatively charged cluster in the former case. However, the present suggestion, while obviously speculative, has the merit of being based on definite structural information, albeit outside of a protein environment, for clusters isoelectronic with the sites of both components of the protein redox couples.

Acknowledgments. This research was supported by Grants NIH GM-22352 and NSF CHE 77-04397 at Stanford University, Grant NIH HL-13157 at Northwestern University, and by the National Science Foundation at the Francis Bitter National Magnet Laboratory. We thank Professor W. M. Reiff and Dr. B. Dockum for assistance with Mössbauer measurements.

Supplementary Material Available: Equations of best weighted least-squares planes of both $[Fe_4S_4(SPh)_4]^{3-}$ anions (Table VI) and values of F_o^2 and F_c^2 for $(Et_3MeN)_3[Fe_4S_4(SPh)_4]$ (Table VIII); appendix containing equations for the magnetic susceptibilities of $[Fe_4S_4(SR)_4]^{2-,3-}$ based on an antiferromagnetic spin coupling model (24 pages). Ordering information is given on any current masthead page.

References and Notes

(1) (a) Stanford University; (b) Francis Bitter National Magnet Laboratory; (c) Swiss National Science Foundation Fellow, 1975-1977; (d) Northwestern University.
(2) (a) W. H. Orme-Johnson, *Annu. Rev. Biochem.*, **42**, 159 (1973); (b) G. Palmer in "The Enzymes", Vol. XII, Part B, 3rd ed, P. D. Boyer, Ed., Academic Press, New York, N.Y., 1975, pp 1-56.
(3) (a) L. H. Jensen, *Annu. Rev. Biochem.*, **43**, 461 (1974); (b) C. W. Carter, Jr., in "Iron-Sulfur Proteins", Vol. III, W. Lovenberg, Ed., Academic Press, New York, N.Y., 1977, Chapter 6.
(4) Abbreviations: Fd, ferredoxin; HMPA, hexamethylphosphoramide; HP, "high-potential" iron-sulfur protein; ox, oxidized; red, reduced; Rd, ru-

bredoxin; S*, acid-labile (sulfide) sulfur (where useful for clarity); s-, "super"; S_2-o-xyl, o-xylyl-α,α'-dithiolate. The HP notation for the protein from *Chromatium* is retained owing to its familiar prior usage. Because the $[Fe_4S_4(S\text{-}Cys)_4]^-$ site oxidation level is apparently no longer unique to this protein,[5,6] it is best considered as a member of the general class of ferredoxins with 4-Fe sites.

(5) (a) W. V. Sweeney, J. C. Rabinowitz, and D. C. Yoch, *J. Biol. Chem.*, **250**, 7842 (1975); (b) D. C. Yoch, R. P. Carithers, and D. I. Arnon, *ibid.*, **252**, 7453 (1977).
(6) (a) R. Cammack, K. K. Rao, D. O. Hall, J. J. G. Moura, A. V. Xavier, M. Bruschi, J. Le Gall, A. Deville, and J.-P. Gayda, *Biochim. Biophys. Acta*, **490**, 311 (1977); (b) J. J. G. Moura, A. V. Xavier, M. Bruschi, and J. Le Gall, *ibid.*, **459**, 278 (1977).
(7) (a) R. H. Holm and J. A. Ibers in ref 3b, Chapter 7; (b) R. H. Holm, *Acc. Chem. Res.*, **10**, 427 (1977).
(8) W. V. Sweeney, A. J. Bearden, and J. C. Rabinowitz, *Biochem. Biophys. Res. Commun.*, **59**, 188 (1974).
(9) (a) R. Cammack, *Biochem. Biophys. Res. Commun.*, **54**, 548 (1973); (b) *J. Phys.* (*Paris*), **37**, C6-137 (1976); (c) *Biochem. Soc. Trans.*, **3**, 482 (1975).
(10) (a) T. Herskovitz, B. A. Averill, R. H. Holm, J. A. Ibers, W. D. Phillips, and J. F. Weiher, *Proc. Natl. Acad. Sci. U.S.A.*, **69**, 2437 (1972); (b) B. A. Averill, T. Herskovitz, R. H. Holm, and J. A. Ibers, *J. Am. Chem. Soc.*, **95**, 3523 (1973).
(11) L. Que, Jr., M. A.Bobrik, J. A. Ibers, and R. H. Holm, *J. Am. Chem. Soc.*, **96**, 4168 (1974).
(12) H. L. Carrell, J. P. Glusker, R. Job, and T. C. Bruice, *J. Am. Chem. Soc.*, **99**, 3683 (1977).
(13) M. A. Bobrik, K. O. Hodgson, and R. H. Holm, *Inorg. Chem.*, **16**, 1851 (1977).
(14) M. A. Bobrik, E. J. Laskowski, R. W. Johnson, W. O. Gillum, J. M. Berg, K. O. Hodgson, and R. H. Holm, *Inorg. Chem.*, **17**, 1402 (1978).
(15) B. V. DePamphilis, B. A. Averill, T. Herskovitz, L. Que, Jr., and R. H. Holm, *J. Am. Chem. Soc.*, **96**, 4159 (1974).
(16) R. B. Frankel, T. Herskovitz, B. A. Averill, R. H. Holm, P. J. Krusic, and W. D. Phillips, *Biochem. Biophys. Res. Commun.*, **58**, 974 (1974).
(17) R. B. Frankel, B. A. Averill, and R. H. Holm, *J. Phys.* (*Paris*), **35**, C6-107 (1974).
(18) R. W. Lane, A. G. Wedd, W. O. Gillum, E. J. Laskowski, R. H. Holm, R. B. Frankel, and G. C. Papaefthymiou, *J. Am. Chem. Soc.*, **99**, 2350 (1977).
(19) J. Cambray, R. W. Lane, A. G. Wedd, R. W. Johnson, and R. H. Holm, *Inorg. Chem.*, **16**, 2565 (1977).
(20) R. W. Lane, J. A. Ibers, R. B. Frankel, G. C. Papaefthymiou, and R. H. Holm, *J. Am. Chem. Soc.*, **99**, 84 (1977).
(21) S. T. Freer, R. A. Alden, C. W. Carter, Jr., and J. Kraut, *J. Biol. Chem.*, **250**, 46 (1975).
(22) See paragraph at end of paper regarding supplementary material.
(23) H. S. Rade, *J. Phys. Chem.*, **77**, 424 (1973).
(24) For means of assessing core geometries cf. ref 10b and C. J. Fritchle, Jr., *Acta Crystallogr., Sect. B*, **31**, 802 (1975).
(25) (a) $Al_4N_4(NPh)_4$: T. R. R. McDonald and W. S. McDonald, *Acta Crystallogr., Sect. B*, **28**, 1619 (1972). (b) $Be_4(OSiMe_3)_4Me_4$: D. Mootz, A. Zinnius, and B. Böttcher, *Angew. Chem., Int. Ed. Engl.*, **8**, 378 (1969). (c) $Zn_4(OMe)_4Me_4$: H. M. M. Shearer and C. B. Spencer, *Chem. Commun.*, 194 (1966). (d) $Cu_4X_4(PEt_3)_4$ (X = Cl, Br): M. R. Churchill, B. G. DeBoer, and S. J. Mendok, *Inorg. Chem.*, **14**, 2041 (1975). (e) $Cu_4I_4(PEt_3)_4$, $Cu_4I_4(AsEt_3)_4$: M. R. Churchill and K. L. Kalra, *ibid.*, **13**, 1899 (1974). (f) $Ag_4I_4(PEt_3)_4$: M. R. Churchill and B. G. DeBoer, *ibid.*, **14**, 2502 (1975); this complex possesses precise D_{2d} symmetry but deviations from idealized T_d symmetry are slight.
(26) C. W. Carter, Jr., J. Kraut, S. T. Freer, R. A. Alden, L. C. Sieker, E. Adman, and L. H. Jensen, *Proc. Natl. Acad. Sci. U.S.A.*, **69**, 3526 (1972).
(27) There are three apparent exceptions to (1). (a) $Ag_4X_4(PEt_3)_4$ (X = Cl, Br): M. R. Churchill, J. Donahue, and F. J. Rotella, *Inorg. Chem.*, **15**, 2752 (1976). (b) $Hg_4(OSIMe_3)_4Me_4$: G. Dittmer and E. Hellner, *Angew. Chem., Int. Ed. Engl.*, **8**, 679 (1969).
(28) (a) $Ag_4Cl_4(PPh_3)_4$: B.-K. Teo and J. C. Calabrese, *Inorg. Chem.*, **15**, 2467 (1976). (b) $Ag_4Br_4(PPh_3)_4$: B.-K. Teo and J. C. Calabrese, *J. Chem. Soc., Chem. Commun.*, 185 (1976). (c) $Ag_4I_4(PPh_3)_4$: B.-K. Teo and J. C. Calabrese, *Inorg. Chem.*, **15**, 2474 (1976). (d) $Cu_4Cl_4(PPh_3)_4$: M. R. Churchill and K. L. Kalra, *ibid.*, **13**, 1065 (1974). (e) $Cu_4I_4(PPh_2Me)_4$: M. R. Churchill and F. J. Rotella, *ibid.*, **16**, 3267 (1977).
(29) (a) $Fe_4S_4(NO)_4$: R. S. Gall, C. T.-W. Chu, and L. F. Dahl, *J. Am. Chem. Soc.*, **96**, 4019 (1974). (b) $Co_4(NC\text{-}t\text{-}Bu)_4(NO)_4$: R. S. Gall, N. G. Connelly, and L. F. Dahl, *ibid.*, **96**, 4017 (1974).
(30) Trinh-Toan, B.-K. Teo, J. A. Ferguson, T. J. Meyer, and L. F. Dahl, *J. Am. Chem. Soc.*, **99**, 408 (1977).
(31) The predictive utility of this model is even more apparent when extended to a variety of $[(\eta^5\text{-}C_5H_5)_4M_4X_4]^z$ complexes, including $[(\eta^5\text{-}C_5H_5)_4Fe_4S_4]^{0,+,2+}$.[30,32]
(32) (a) Trinh-Toan, W. P. Fehlhammer, and L. F. Dahl, *J. Am. Chem. Soc.*, **99**, 402 (1977); (b) R. A. Schunn, C. J. Fritchle, Jr., and C. T. Prewitt, *Inorg. Chem.*, **5**, 892 (1966); C. H. Wei, G. R. Wilkes, P. M. Treichel, and L. F. Dahl, *Ibid.*, **5**, 900 (1966).
(33) E. T. Adman, L. C. Sieker, and L. H. Jensen, *J. Biol. Chem.*, **248**, 3987 (1973); **251**, 3801 (1976).
(34) C. W. Carter, Jr., J. Kraut, S. T. Freer, and R. A. Alden, *J. Biol. Chem.*, **244**, 6339 (1974).
(35) (a) C. Y. Yang, K. H. Johnson, R. H. Holm, and J. G. Norman, Jr., *J. Am. Chem. Soc.*, **97**, 6596 (1975). Note that the results reported refer to $[Fe_4S_4(SMe)_4]^{2-}$; calculations have not been performed for other species with R ≠ H. (b) K. H. Johnson, private communication, Oct 1977.
(36) R. W. Jotham and S. F. A. Kettle, *Inorg. Chim. Acta*, **5**, 183 (1971).
(37) The normal modes of M_4X_4 in T_d symmetry span the representations $2A_1 + 2E + T_1 + 3T_2$. The forms of these modes are obtainable from those of cubic MX_8 (cf., e.g., A. D. Liehr, *J. Phys. Chem.*, **67**, 389 (1963); *Prog. Inorg. Chem.*, **3**, 281 (1962)).
(38) J. M. Berg, K. O. Hodgson, and R. H. Holm, results to be published.
(39) S. G. Mayhew, D. Petering, G. Palmer, and G. P. Foust, *J. Biol. Chem.*, **244**, 2830 (1969); K. Uyeda and J. C. Rabinowitz, *ibid.*, **246**, 3111 (1971).
(40) N. A. Stombaugh, R. H. Burris, and W. H. Orme-Johnson, *J. Biol. Chem.*, **248**, 7951 (1973).
(41) R. N. Mullinger, R. Cammack, K. K. Rao, D. O. Hall, D. P. E. Dickson, C. E. Johnson, J. D. Rush, and A. Simopoulos, *Biochem. J.*, **151**, 75 (1975).
(42) R. Mathews, S. Charlton, R. H. Sands and G. Palmer, *J. Biol. Chem.*, **249**, 4326 (1974).
(43) R. E. Anderson, G. Anger, L. Petersson, A. Ehrenberg, R. Cammack, D. O. Hall, R. Mullinger, and K. K. Rao, *Biochim. Biophys. Acta*, **376**, 63 (1975).
(44) (a) L. Que, Jr., J. R. Anglin, M. A. Bobrik, A. Davison, and R. H. Holm, *J. Am. Chem. Soc.*, **96**, 6042 (1974); (b) C. L. Hill, J. Renaud, R. H. Holm, and L. E. Mortenson, *ibid.*, **99**, 2549 (1977).
(45) R. H. Holm, B. A. Averill, T. Herskovitz, R. B. Frankel, H. B. Gray, O. Siiman, and F. J. Grunthaner, *J. Am. Chem. Soc.*, **96**, 2644 (1974).
(46) C. L. Thompson, C. E. Johnson, D. P. E. Dickson, R. Cammack, D. O. Hall, U. Weser, and K. K. Rao, *Biochem. J.*, **139**, 97 (1974).
(47) R. Cammack, D. P. E. Dickson, and C. E. Johnson in ref 3b, Chapter 8.
(48) P. Middleton, D. P. E. Dickson, C. E. Johnson, and J. D. Rush, results to be published.
(49) Computer program by B. L. Chrisman and T. A. Tumolillo, Technical Report No. 178, Department of Physics, University of Illinois, Urbana, Ill.
(50) R. B. Frankel, G. C. Papaefthymiou, R. W. Lane, and R. H. Holm, *J. Phys.* (*Paris*), **37**, C6-165 (1976).
(51) J. J. Mayerle, R. B. Frankel, R. H. Holm, J. A. Ibers, W. D. Phillips, and J. F. Weiher, *Proc. Natl. Acad. Sci. U.S.A.*, **70**, 2429 (1973).
(52) D. P. E. Dickson, C. E. Johnson, R. Cammack, M. C. W. Evans, D. O. Hall, and K. K. Rao, *Biochem. J.*, **139**, 105 (1974).
(53) D. P. E. Dickson and R. Cammack, *Biochem. J.*, **143**, 763 (1974).
(54) A. Kostikas, V. Petrouleas, A. Simopoulos, D. Coucouvanis, and D. G. Holah, *Chem. Phys. Lett.*, **38**, 582 (1976).
(55) W. M. Reiff, I. E. Grey, A. Fan, Z. Eliezer, and H. Steinfink, *J. Solid State Chem.*, **13**, 32 (1975).
(56) Other contributing factors to the overall spectral complexity include different magnitudes and directions of the magnetic hyperfine interactions at the two sites, different quadrupole interactions, randomization in the polycrystalline samples of the angle between the principal component of the electric field gradient and the magnetic hyperfine field, and possible asymmetries in both the quadrupole and magnetic hyperfine interactions.
(57) P. Middleton, J. D. Rush, D. P. E. Dickson, R. B. Frankel, and G. C. Papaefthymiou, results to be published.
(58) D. P. E. Dickson, C. E. Johnson, C. L. Thompson, R. Cammack, M. C. W. Evans, D. O. Hall, K. K. Rao, and U. Weser, *J. Phys.* (*Paris*), **35**, C6-343 (1974).
(59) As noted by Cammack et al.[47] this model is apparently inconsistent with the results of ENDOR spectroscopy ($\tau \sim 10^{-9}$ s) which has not detected inequivalent sites in native and unfolded *C. pasteurianum* Fd_{red} or in HP_{red}.[43]
(60) This observation eliminates the remote possibility that the pairs of quadrupole doublets in the two polycrystalline salts of $[Fe_4S_4(SPh)_4]^{3-}$ arise from crystallographically inequivalent anions.
(61) One precedent is found with Eu_3S_4: O. Berkooz, M. Malamud, and S. Shtrikman, *Solid State Commun.*, **6**, 185 (1968).
(62) Incipient magnetic hyperfine structure arising from electronic relaxation times of the order of the nuclear Larmor precession time could produce the observed line widths, in which case the fast exchange limit may have been reached.
(63) (a) J. K. Beattie, N. S. Hush, P. R. Taylor, C. L. Raston, and A. H. White, *J. Chem. Soc., Dalton Trans.*, 1121 (1977). (b) Contrast the case of the Ru dimer and $[Fe_4S_4(SR)_4]^{3-}$, in which individual atom formal oxidation states differ by virtue of the number of essentially nonbonding d electrons, with a mixed valence complex where antibonding d electrons are involved, e.g., $[Mn_2O_2(bipyridyl)_4]^{3+}$: P. M. Plaskin, R. C. Stoufer, M. Mathew, and G. J. Palenik, *J. Am. Chem. Soc.*, **94**, 2121 (1972).
(64) W. E. Hatfield in "Theory and Applications of Molecular Paramagnetism", E. A. Boudreaux and L. N. Mulay, Ed., Wiley-Interscience, New York, N.Y., 1976, Chapter 7.
(65) B. C. Antanaitis and T. H. Moss, *Biochim. Biophys. Acta*, **405**, 262 (1975).
(66) M. Cerdonio, R.-H. Wang, J. Rawlings, and H. B. Gray, *J. Am. Chem. Soc.*, **96**, 6534 (1974).
(67) G. B. Wong, M. A. Bobrik, and R. H. Holm, *Inorg. Chem.*, **17**, 578 (1978).
(68) Any such impurities present would be masked by the paramagnetism of the trianions. EPR spectra of trianion salts in frozen solutions showed only very weak signals at $g \sim 4.3$ compared with the majority resonances (Table X), suggesting little contamination from high-spin Fe(III).
(69) J. G. Reynolds, E. J. Laskowski, and R. H. Holm, *J. Am. Chem. Soc.*, preceding paper in this issue.
(70) W. D. Phillips, C. C. McDonald, N. A. Stombaugh, and W. H. Orme-Johnson, *Proc. Natl. Acad. Sci. U.S.A.*, **71**, 140 (1974).
(71) E. Adman, K. D. Watenpaugh, and L. H. Jensen, *Proc. Natl. Acad. Sci. U.S.A.*, **72**, 4854 (1975).
(72) C. W. Carter, Jr., *J. Biol. Chem.*, **252**, 7802 (1977).
(73) N. A. Stombaugh, J. E. Sundquist, R. H. Burris, and W. H. Orme-Johnson, *Biochemistry*, **15**, 2633 (1976); E. T. Lode, C. L. Murray, and J. C. Rabinowitz, *J. Biol. Chem.*, **251**, 1683 (1976).
(74) Cf., e.g., S. G. Mayhew, D. Petering, G. Palmer, and G. P. Foust, *J. Biol. Chem.*, **244**, 2830 (1969).
(75) J. J. Hopfield, *Proc. Natl. Acad. Sci. U.S.A.*, **71**, 3640 (1974).
(76) J. Peisach, N. R. Orme-Johnson, W. B. Mims, and W. H. Orme-Johnson, *J. Biol. Chem.*, **252**, 5643 (1977).